INVESTIGATION OF NEGATIVE RESISTANCE INDUCED BY DIRECTIONAL
SCATTERING IN A TWO DIMENSIONAL ELECTRON GAS

by

Engin Karabudak

Submitted to the Graduate School of Engineering and Natural Sciences
in partial fulfillment of
the requirements for the degree of
Master of Science

Sabanci University
Summer 2006

INVESTIGATION OF NEGATIVE RESISTANCE INDUCED BY DIRECTIONAL
SCATTERING IN A TWO DIMENSIONAL ELECTRON GAS

Engin KARABUDAK

Faculty of Engineering and Natural Sciences, MSc Thesis, 2006

Thesis Supervisor: Assoc. Prof. Ismet I. Kaya

Abstract

In the last decades, it became possible to manufacture high mobility two-dimensional conductors. The study of electron transport in such two dimensional conductors has led to discovery of many new physical phenomena, two of which were awarded with Nobel prizes. The reduction in the dimensions of a conductor drastically changes the scattering properties of carriers. Intercarrier scattering angle is also severely reduced in two dimensions. Recently, it was shown that this kind of directional scattering can be exploited to achieve electron multiplication and absolute negative resistance in a three terminal configuration. Experimental results suggest that such an effect should boost as the device size shrinks and can be useful to fabricate compact high frequency sources that are not yet within the reach of conventional semiconductor devices.

The purpose of this thesis is to extend further the experimental study of such phenomena, and in particular, to understand its dependence on the device size. For this a new fabrication method has been developed. This method gives a greater flexibility to shrink the device size down to sub-microns. The new generation of fabricated devices produce high electron multiplication ratios up to 5.

IKI BOYUTLU ELEKTRON GAZINDA YÖNELMIS SAÇILMADAN
KAYNAKLI EKSI DIRENCIN INCELENMESI

Engin KARABUDAK

MDBF, Master Tezi, 2006

Tez Danismani: Doç. Dr. Ismet I. Kaya

Özet

Yakin geçmiste yüksek hareketlilikli iki boyutlu iletkenlerin üretilmesi mümkün olmustur. Bu iki boyutlu iletkenlerde yapilan çalismalar, ikisi Nobel ödülü alan birçok yeni fiziksel olayin kesfine yolaçmistir. Boyut sayisindaki azalmayla elektron saçilma nitelikleri çok degismekte ve elektron-elektron çarpisma açisi çok daralmaktadir. Yakin zamanlarda, bu tür yöneltilmis saçilmalarin iki boyutta, elektron çogalmasina ve mutlak eksi direnç elde edilmesinde kullanilabilecegi gösterilmistir. Deneyler aygit boyutlari daha da küçüldügünde bu etkinin güçlenecegini göstermekte ve yeni bir THz radyasyon kaynagi yapiminda kullanma olasiligini göstermektedir.

Bu tezin ana amaci, deneysel olarak daha da küçültülmüs, elektron çogaltma aygiti üretme metodu gelistirmek ve üretilen aygitlarin elektriksel özelliklerini boyutlarina bagli olarak incelemektir. Bu yeni üretim metodu aygit boyutlarinin mikron alti büyüklüklere indirilebilmesini mümkün kilmaktadir. Bu çalismada üretilen 2 mikron baz uzunlugundaki aygitin akim transfer oranin 5'e kadar çikabildigi gözlenmistir.

Acknowledgements

TABLE OF CONTENTS

LIST OF FIGURES

Chapter 1

INTRODUCTION

1.1. Motivation

Earlier experiments done by I. I. Kaya [1,2] demonstrated absolute negative resistance in a three terminal device fabricated on a AlGaAs/GaAs two dimensional electron gas (2DEG). The layout of the device is shown in Figure 1.1. The device exploits the enhanced directionality of electron-electron scattering angle in two dimensions to achieve current reversal or potential depression in the middle contact of a three terminal device. Results suggest enhancement of the effect in smaller devices. Fabrication of a smaller device (~ 1 µm in base length) is needed in order to improve negative resistance. The main motivation of this thesis is to develop a new fabrication method to achieve smaller device dimensions and characterize them to understand the size effects. Using this new method is more efficient and simpler. A device with 2 µm base length has been fabricated and characterized.

1.2. Two Dimensional Electron Gas

Since electrons are fermions, they obey the Fermi-Dirac statistics. Their energy distribution function is:

$$f_0(\varepsilon) = \frac{1}{\exp[(\varepsilon - \mu)/kT] + 1} \tag{1.1}$$

where μ is the chemical potential, e is the energy, k is the Boltzman constant and T is the temperature.
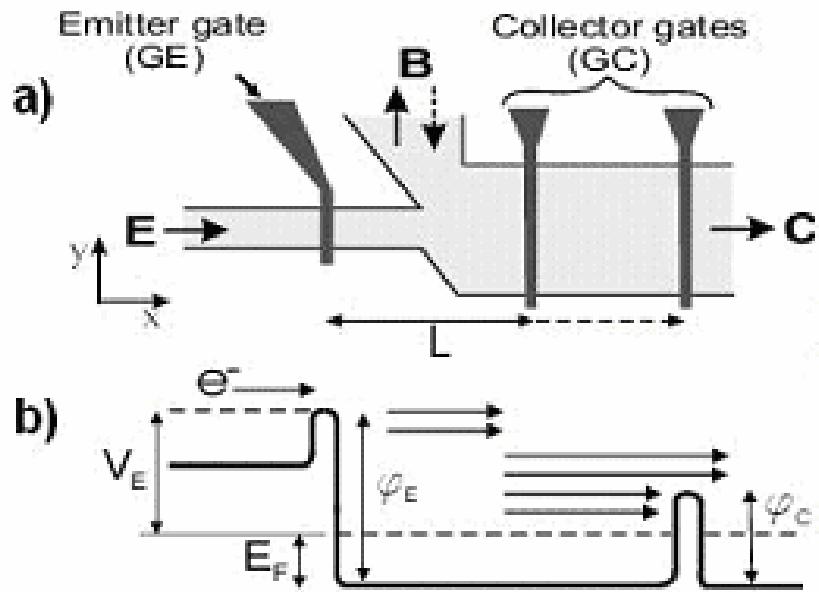
Figure 1.1 : Hot Electron Device in 2DEG[1],

a) Schematics and b) Energy diagram of the device.
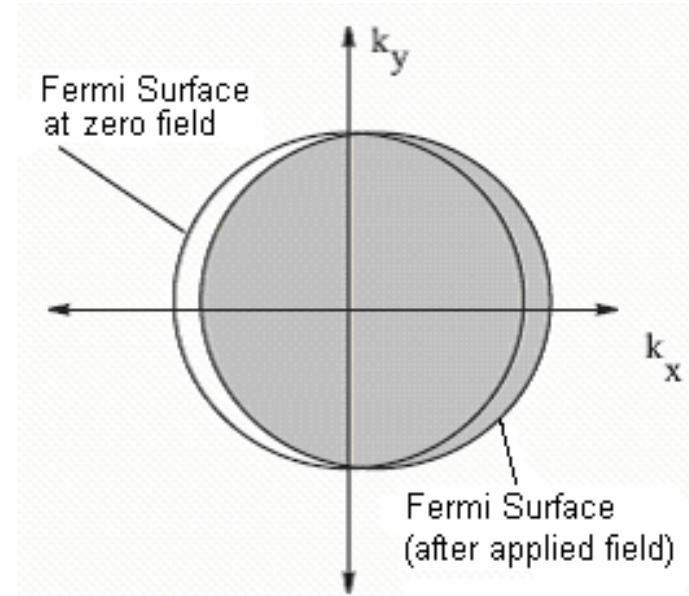
Figure 1.2 : Fermi circle of a 2DEG under applied electric field.

In two dimensional systems, electrons form a circular Fermi surface (see Figure 1.2). With the application of an electric field, Fermi surface shifts in the direction of

the field applied. The shift of the Fermi surface results asymmetric charged particle distribution. Asymmetry causes a potential in the opposite direction. This is called Coulomb potential [3]. If there is no dominant phonon scattering, system tries to relax to a symmetric distribution due to the electron-electron (e-e) scattering mechanism. This process is called momentum relaxation [4].

At low temperatures, electron-electron scattering mechanism is the only momentum relaxation process. If a high energy electron is scattered with a low energy electron, both electrons must have energies outside the Fermi circle, due to Pauli Exclusion Principle. This restricts the scattering angle severely in 2DEG compared to 3D conductors.

In this system, e-e scattering angle is restricted by Pauli's Exclusion Principle, energy conservation and momentum conservation. Therefore, e-e scattering in a two dimensional system is a small angle process [5]. In other words, e-e scattering is directional in 2DEG.

1.3. AlGaAs / GaAs Two Dimensional Electron Gas (2DEG)

1.3.1. AlGaAs / GaAs 2DEG

In 1978, R. Dingle *et al.* [6], reported the first modulation doped AlGaAs / GaAs superlattice structure. Molecular beam epitaxy (MBE) is used to produce atomically smooth layers of GaAs and $Al_xGa_{1-x}As$ superlattice. Today, the system is known as AlGaAs / GaAs 2DEG. Figure 1.3 shows the band structure of a generic 2DEG. In modulation doped superlattice, all carriers and their donor impurities are separated from each other, so that high mobility can be reached.

There is a conduction band energy difference of 0.3 eV between GaAs and AlGaAs. Therefore, when an epitaxially thin and clean layer AlGaAs is grown on GaAs, there is a formation of triangular potential. At low temperatures, conduction electrons from donor impurities cool down to triangular potential barriers. Energy quantization occurs in this triangular potential well in one direction. Therefore, electrons have mobility only in two dimensions. Two dimensional transport properties are different in comparison to three dimensional transport [5].
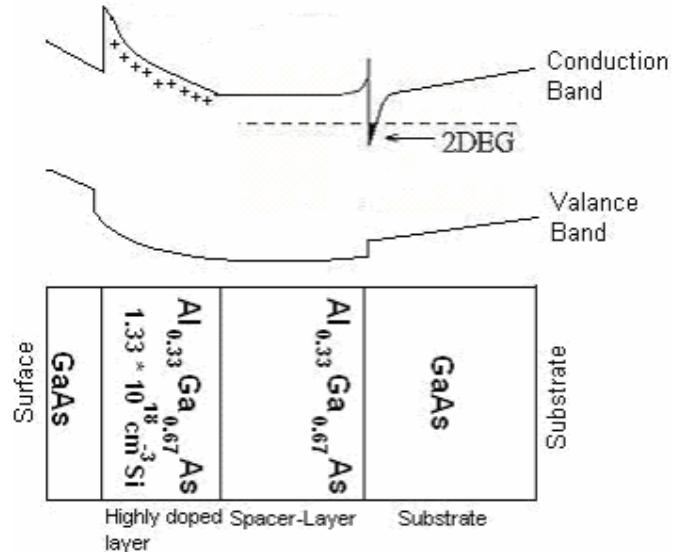
Figure 1.3: Band Structure of the interface between n-AlGaAs and intrinsic GaAs. Excess electrons condense in the triangular well and form the 2DEG when cooled to cryogenic temperatures [7].
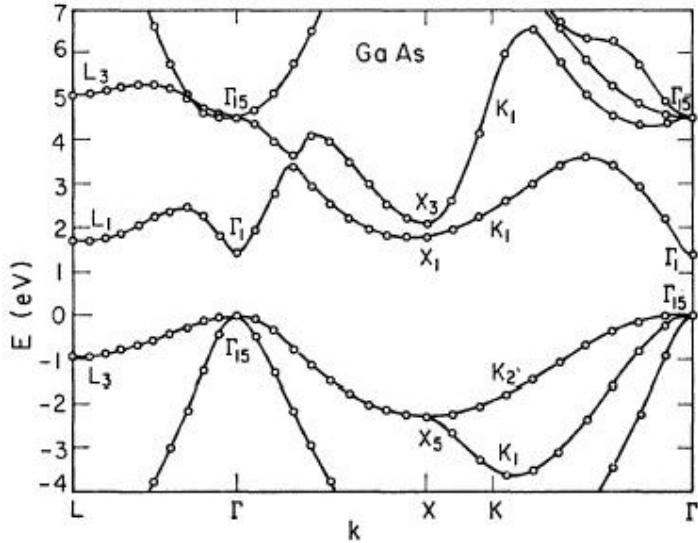
Figure 1.4: Band Structure of GaAs [8].

Two dimensional electron gas is formed between GaAs and AlGaAs layers. This system has three main advantages for experimental work:

i) Electron mobility in AlGaAs/ GaAs 2DEG is higher than bulk GaAs, because the donors that supply the electrons are located in a remote region of the wafer which does not contain impurity [6]. Therefore, electron impurity scattering rate is reduced.

ii) 2DEG has very low carrier density. Therefore, electron densities can be controlled by applied electric field via metallic gates placed on the surface. When a negative potential is applied to the surface metallic gate, gate potential depletes the area below. Therefore, the carrier density changes. Electron density under biased gate is

$$N = m^* (E_F - F) / p \hbar^2 \qquad (1.2)$$

where E_F is the Fermi Energy; N is the electron density under the biased gate; F is the electrostatic potential under the gate due to basing and, m^* is the effective electron mass [9].

J. Spector *et al.* [10] used surface lithographic gates in order to construct refractive prism for ballistic electron beams. L.W. Molenkamp *et al.* [11] collimated the electron beam by point contact. B. J. van Wees *et al.* [12] showed the conductance quantization of a point contact.

iii) Two dimensional electron gas can be shaped by etching. Etching of 2DEG, helps the formation of predefined two dimensional conductors.

In this thesis, one sample of 2DEG structures has been used.

Sample 8789 which was grown by Karl Eberl at MPI-FKF in Stuttgart, has the mobility of $\mu = 9.0 \times 10^5$ cm^2 / V . s and the sheet electron density of $N_s = 2 \times 10^{11}$ cm^{-2} at 4.2 K. The mobility is related to mean free time between the scattering events via Drude conductance formula:

$$\mu = \frac{e\tau}{m^*} \qquad (1.3)$$

where m* is the effective mass of electron for GaAs ($m^* = 0.067$ m$_e$) (m$_e$ is free electron mass), e is electron's charge, t is average inelastic scattering time. (t = 3.4 x 10^{-11} s for 8789);

In two dimensions, density of states is:

$$\rho_{2D} = \frac{m^*}{\pi \hbar^2} \qquad (1.4)$$

For $k_B T << E_F$; Fermi energy and Fermi velocity are given as

$$E_F = N_s / \rho_{2D} \qquad (1.5)$$

where k_B is Boltzman constant, T is temperature in Kelvin.

$$v_F = \sqrt{\frac{2\,E_F}{m^*}} \qquad\qquad (1.6)$$

Inelastic mean free path is defined as

$$l_{mfp} = v_F \ \text{x} \ \ t \qquad\qquad (1.7)$$

These values for sample 8789 are calculated as $E_F = 7.1$ meV, $v_F = 1.9$ x 10^5 m / s and $l = 6.6$ μm.

Electron transport is ballistic for dimensions smaller than inelastic mean free path. Ballistic devices show different characteristics than usual diffusive devices (see [9][13][14]).
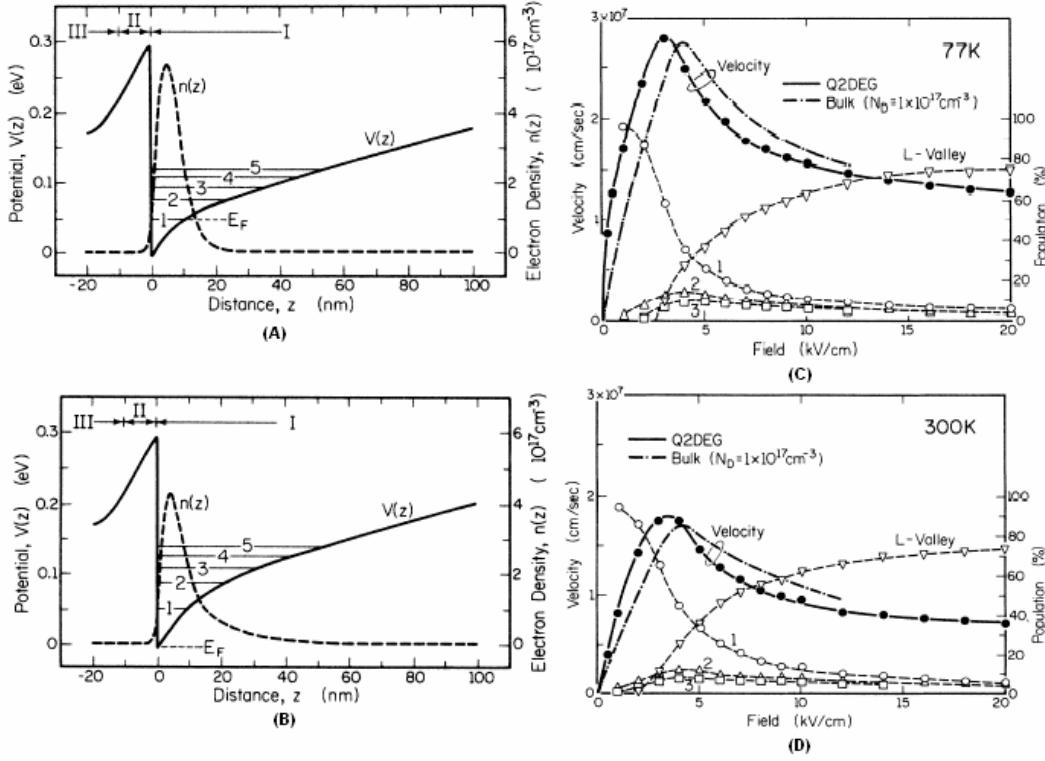
Figure 1.5 : Calculated effective potentials, electron densities of 2DEG and velocities of electrons in 2DEG (left). Calculated effective potential and electron density distribution of 2DEG (a) 77 K , (b) 300 K, (right) Steady state velocity and population of electrons versus electric field that is applied, characteristics at (c) 77 K and (d) 300 K. From Kiyoyuki and Hess [15] .

1.3.2. Transport Properties of AlGaAs / GaAs 2DEG

Yokoyama and Hess [15] calculated electronic multisubband states and transport properties of single well AlGaAs/GaAs 2DEG. During the calculations five lowest subbands are being considered. (Electron densities of subbands at 77 K and 300 K are seen in Figure 1.5 (a) and (b)). Electron velocities and electron occupation numbers in subbands including L-valley, are calculated. The results are shown in Figure 1.5 (c) and (d). Here, the electron population in L-valley at higher fields is noticeable.

Scattering mechanisms that limits the electron mobility in AlGaAs / GaAs 2DEG, can be divided in two groups as extrinsic and intrinsic [14] . Extrinsic effects are charged impurity scatterings. They are result of unintentional doping of bulk GaAs and AlGaAs spacer layers. Improvements in growth and fabrication techniques can reduce extrinsic effects.

Intrinsic effects are remote ionized impurity scattering and lattice phonons. Remote ionized impurity scattering is a result of highly doped AlGaAs layer. Remote ionized impurity can be reduced by the presence of undoped AlGaAs spacer layer between GaAs and doped AlGaAs.
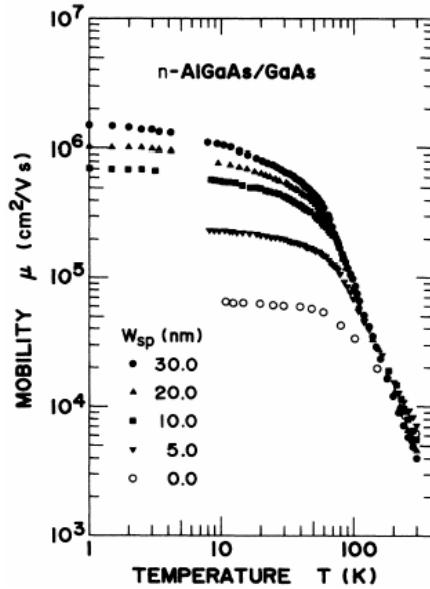
Figure 1.6 : Mobility of 2DEGs with different spacer layer width versus temperature [17].

Figure 1.6 from Hirakawa and Sakaki [17] , displays the mobility versus temperture for 2DEG structures with different spacer layer thicknesses.

Phonon scattering also limits the conductance [16]. Phonon scattering can not be reduced, because phonon scattering is the intrinsic property of all atomic crystals. Kawamura and Sarma [16] calculated the phonon scattering contribution in range of 1-300 K, with variational-subband-wave-function model and with Random Phase Approximation (RPA). They assumed lowest subband occupation for calculations. Results imply three physically distinct regions. Bloch-Gruneisen (BG) region (0 – 4 K), equipartition region (EP) (4 - 40 K), inelastic regime (above 40 K) are expressed. In BG region, effect of acoustic phonons and thermal energy is comparable, therefore instead of phonons, remote ion scattering limits the electron mobility. In equapartition region, electron mobility is limited by deformation-potential coupled acoustic phonons and piezoelectric coupled acoustic phonons. In this regime, thermal energy is higher than acoustic phonons, which means electron scattering is quasi-elastic. In inelastic region, LO phonons contribute to electron mobility, which results in inelastic scattering of electrons.

Developments in molecular beam epitaxy (MBE) led to an immediate improvement in mobility of AlGaAs / GaAs 2DEG. Mobilities in the order of 10^7 cm^2 / V-s can be achieved in cryogenic temperatures [18]. Figure 1.7 shows the improvement of mobility from 1978 [6] to 1989 [18].
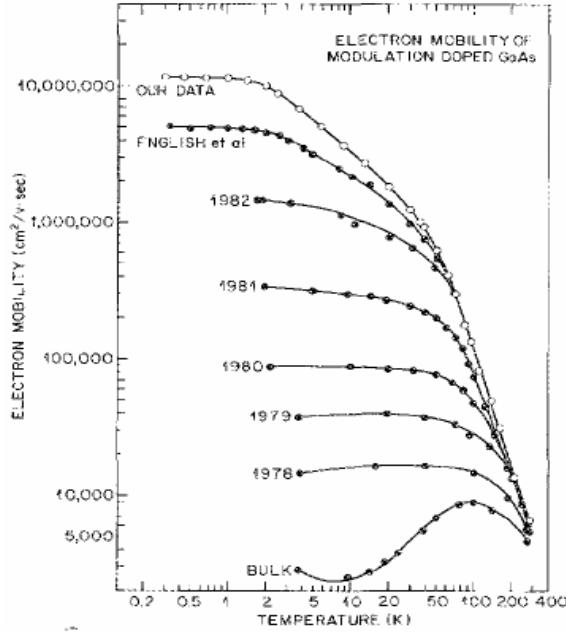
Figure 1.7: Hall mobility of some landmark samples in history from Ref . [18].

1.3.3. Quasiparticle Lifetime in AlGaAs / GaAs 2DEG

In BG regime of temperature, electron mean free path is determined by remote ion scattering [16]. Electron transport is influenced by elastic electron-electron scattering. Elastic electron-electron scattering does not change the total momentum, whereas, elastic electron-electron scattering determines the quasi particle lifetime. Inelastic Coulomb lifetime t_{ee} is an important parameter for the behavior of 2DEG systems at low temperatures.

Boltzmann Transport Equation (BTE) [7] must be solved in order to calculate the scattering lifetime.

$$\frac{\partial f}{\partial t} + v\frac{\partial f}{\partial r} \;-\; e\,(E + \frac{1}{c}[\mathbf{v} \times \mathbf{H}])\,\frac{\partial f}{\partial p} \;=\; \frac{\partial f}{\partial t}\Big|_{coll} \qquad (1.8)$$

$f(p,r)$ is the non-equilibrium distribution function and p is the momentum; r is the position, v is the velocity, $\mathbf{E}$ is the electric field and $\mathbf{H}$ is the magnetic field.

Analytical solution of Boltzmann Transport Equation is not possible for realistic systems. Therefore, approximation methods are used to calculate t_{ee}. Giuliani and Quinn [3], used perturbative approach based upon the random-phase approximation in order to calculate t_{ee} in two dimension (see Eq 1.9. and Eq 1.10).

$$\frac{1}{\tau_{ee}(\Delta)}\Big|_{e-h} = -\frac{E_F}{4\,\pi\,\hbar}\left(\frac{\Delta}{E_F}\right)^2 \left(\ln\left(\frac{\Delta}{E_F}\right) - \frac{1}{2} - \ln\left(\frac{2q_{TF}^{(2)}}{p_F}\right)\right) \;,\; T = OK\,,\, \Delta << \frac{\hbar^2\,p_F\,q_{TF}^{(2)}}{m} \quad (1.9)$$

$$\frac{1}{\tau_{ee}(\Delta)}\Big|_{e-h} = -\frac{E_F}{2\,\pi\,\hbar}\left(\frac{k_B T}{E_F}\right)^2 \left(\ln\left(\frac{k_B T}{E_F}\right) - \ln 2 - \ln\left(\frac{2q_{TF}^{(2)}}{p_F}\right) - 1\right) \;,\; \Delta << k_B T << E_F \qquad (1.10)$$

where Δ is the small excitation energy, p_F is the fermi momentum, t_{ee} is inelastic coulomb lifetime and $q_{TF}^{(2)}$ is the Thomas – Fermi screening wave vector in two dimensions.

Equations 2.2 and 2.3 are successful while interpreting the experimental results of various studies [19][20][21][22][23][24][25].

Guiliani and Quinn [3] calculated the electron-plasmon excitations at zero temperature. They concluded that there is a finite excitation energy threshold Δ_c for decay into plasmon.

$$\Delta_C = \left(\frac{32 \, m \, e^2 \, E_F \, (E_F + \Delta_C)^{1/2}}{3 \, \hbar} \right)^{1/2} \cos \left(\frac{p}{3} + \frac{1}{3} \arccos \left(\frac{E_F + \tilde{\Delta}(r_S)}{E_F + \Delta_C} \right)^{3/4} \right) \tag{1.11}$$

where $\tilde{\Delta}(r_S) = \left(\left(\frac{r_S}{0.42} \right)^{2/3} - 1 \right) E_F$; r_s is the average interelectronic distance measured in

Bohr radii.

Fukayama and Abrahams [26] evaluated diffusion propagator diagrammatically in two dimensional metals in the existence of inelastic scattering due to screen Coulomb interactions.

$$\frac{1}{\tau_e} = \begin{cases} \dfrac{\pi \, T^2}{2 \, E_F} \ln \dfrac{E_F}{T}, & T > 1/\tau \\[2ex] \dfrac{T}{2 \, E_F \, \tau} \ln \dfrac{T_1}{T}, & T < 1/\tau \end{cases} \tag{1.12}$$

where τ_e is the inelastic scattering lifetime and τ is the elastic scattering lifetime,

$T_1 = 4 \, (E_F \, \tau)^2 \, D \, \kappa^2$; $\kappa = 2 \, m \, e^2$; $D = v_F^2 \, \tau / 2$.
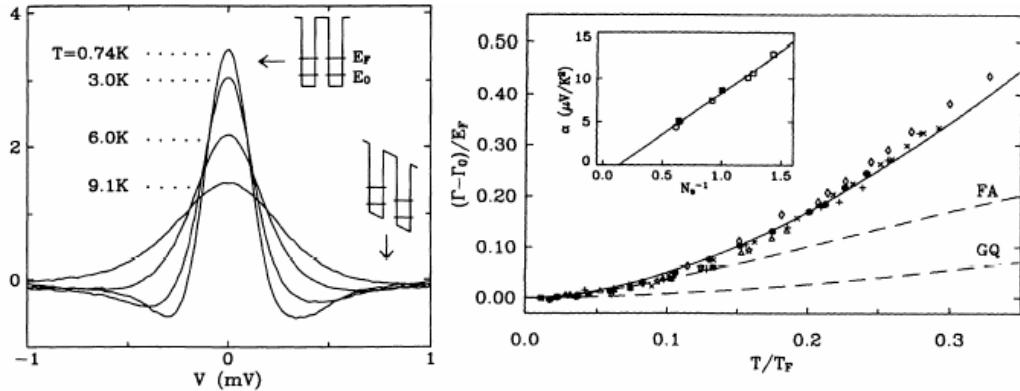
Figure 1.8 : Tunneling electrons between two-dimensional electron systems from Murphy *el al.* [27] (left): typical 2D-2D tunneling resonances observed at various temperatures in a sample with equal electron density (Ns = 1.6 x 10^{11} cm^{-2}) in the two 2DES's. Inset show simplified band diagrams on and off resonance. (right): Tunneling resonance width vs temperature for all samples (having eight different densities). On dividing T by T_F and the resonance width (minus the zero temperature limit G_0 (linewidth) by E_F all the data collapse onto single curve. The dashed lines are the calculations of GQ [3] and FA [26].

Murphy *el al.* [27] used tunneling electrons between two-dimensional electron systems, in order to measure quasiparticle lifetime of electrons. Different temperatures give different tunneling resonances. (Figure 1.8.a) Linewidth is measured at half width at half maximum. Due to Heisenberg Uncertainty principle, electron lifetime is calculated from linewidth (G). Results showed a factor of 6 disagreement with the theory [3] (Figure 1.8b).
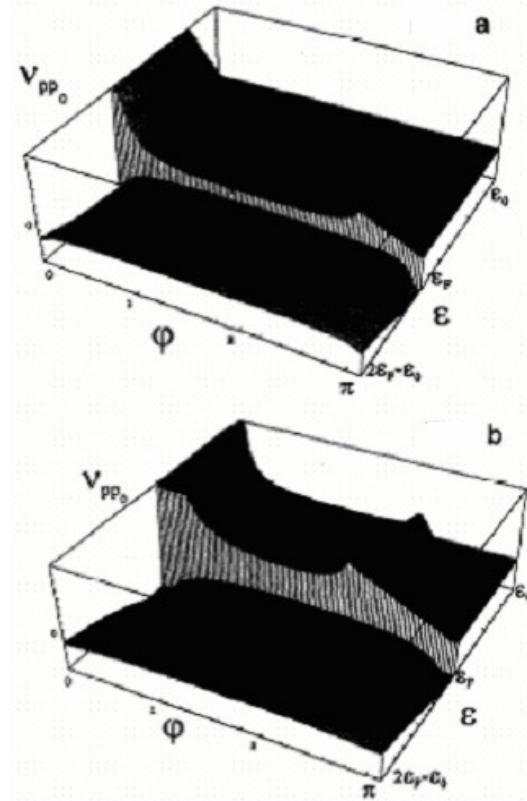
Figure 1.9 : Dependence of the response function v on the energy e and angle, f : (a) $\epsilon = 0.1$; (b) $\epsilon = 0.32$; where $\epsilon = (e_0 - \epsilon_F) / \epsilon_F$, From Ref. [34] .

Lian Zheng and S. Das Sarma [28] tried to understand the discrepancy between Giuliani and Quinn calculations [2] and Murphy *et al.* [27]. They calculated t_{ee} using a single loop dynamically screened Coulomb interaction within random-phase approximation. It is claimed that reason is due to missing $(p/2)^2$ in Eq 1.13. Their asymptotic results [15] are shown Eq. 1.13 and Eq. 1.14.

$$\left. \frac{1}{\tau_{ee}(T)} \right|_{e-h} = -\frac{\pi E_F}{8\hbar} \left(\frac{k_B T}{E_F} \right)^2 \left(\ln\left(\frac{k_B T}{E_F} \right) \right) \quad for \ \ E_F \gg k_B T \gg \Delta \qquad (1.13)$$

$$\left.\frac{1}{\tau_{ee}(\Delta)}\right|_{e-h} = -\frac{E_F}{4\pi\hbar}\left(\frac{\Delta}{E_F}\right)^2\left(\ln\left(\frac{\Delta}{E_F}\right)\right) \quad for \quad E_F >> \Delta >> k_B T \qquad (1.14)$$

Equation 1.13. is in excellent agreement with tunneling experiments results of Murphy *et al.* [27].

1.4. Electron – Electron Scattering Angle in AlGaAs / GaAs 2DEG

Electron- electron scattering in two dimensional systems is shown to be a small angle process. That is proved in many studies [29][30][31][32][33].
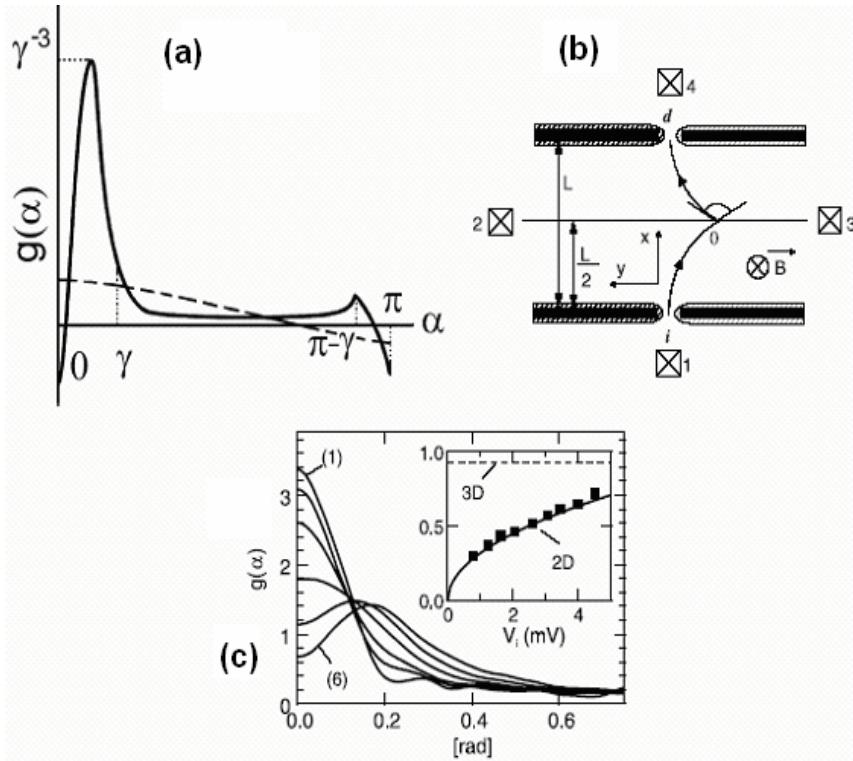
Figure 1.10 : Schematic and measurement results of device that is fabricated by Yanovsky *et al.* [30]. (a) The schematic view of the e-e scattering indicatric g(a) in a 2D system (solid line); dashed line is the 3D case. (b) Layout of the device, *i: injecter; d:detector;* O: scattering point;   (c) e-e scattering indicatrix g(a) obtained from experiment (1) V_i = -0.8 mV , (2) -1.2 mV, (3) -2.06 mV, (4) -2.3 mV, (5) -3.5 mV, (6) -3.8 mV, Inset: small angular peak width da (squares) as a function of V_i.From Ref. [30].

Buhmann *et al.* [34] calculated the electron-electron scattering mechanism in 2D degenerate systems both analytically and numerically (Figure 1.9). The result shows the directional scattering theoretically. In Figure 1.9, response function ν is the probability of e-e scattering. Angle f is the angle between scattering electrons. ϵ_F is Fermi energy of the system and e_0 is the energy of non-equilibrium electron that is scattered.

Yanovsky *et al.* [30] tried to show small angular process experimentally. In Figure 1.10.a, |g(a)|da characterizes the probability of scattering theoretically. The scattering angle is shown as a. Their sample has $n_s = 2.8 \times 10^{11}$ cm^{-2} and $l_{mfp} = 10$ μm. Figure 1.10.a shows the theoretical plot. Experimental results can be seen in Figure 1.10.c. Inset of Figure.1.10.c shows the angular peak width versus injection energy.

1.5. Lateral Hot Electron Devices in AlGaAs / GaAs 2DEG

1.5.1. Lateral Tunneling Electron Spectroscopy
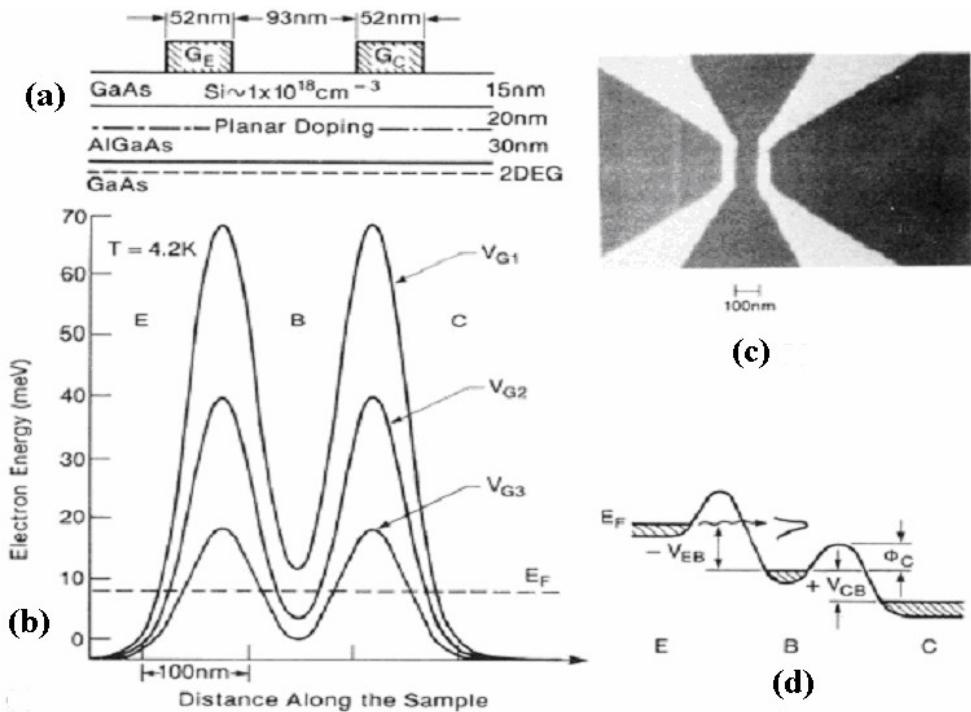
Figure 1.11 : Lateral tunneling electron spectroscopy; (a) At top, Layout of the device (b) Energy diagram of the device (c) SEM picture of the device. (d) A schematic description of the potential distribution for a biased device, $V_{EB} < 0$ and $V_{CB} > 0$. From Palevski *et al.* [35].

Palevski *et al.* [35] demonstrated the lateral tunneling in a two depleted barrier system. V_{EB} and V_{CB} are the barrier height of barriers. Hot electrons are tunneled from one electrostatic barrier (injector) and energy spectrum of electrons (spectrometer) are detected by tuning the second barrier (see Figure 1.11.d). They detected narrow injected electron distribution which was the same as injected electrons. Direct ballistic transport is verified (see Figure 1.12).

1.5.2. Hot Ballistic Transport

Sivan *et al.* [13] tried to investigate the hot-electron transport and its dependence to injection energy. Hot electrons that have energy below LO-phonon emission (36 meV) have reached 2 µm ballistic transport length, which is an order of magnitude longer than theoretical electron-hole excitation [36] and more than electron plasmon scattering [37]. Oscillation in the periods of LO-phonon emission is observed. (See Figure 1.13.)
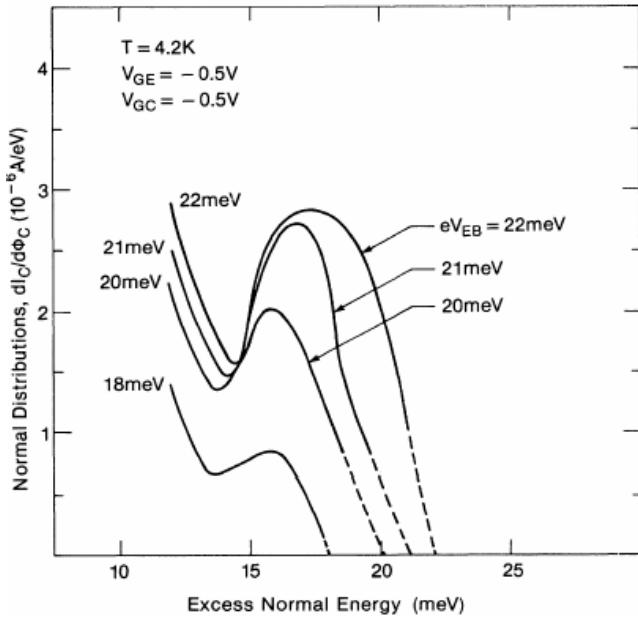
Figure 1.12: The ballistic distribution of electrons for different injection energies as a function of excess normal energy above the Fermi Level in the base from Palevski et al. [35]. The peaks of the distributions follow rigidly the injection energy.

14
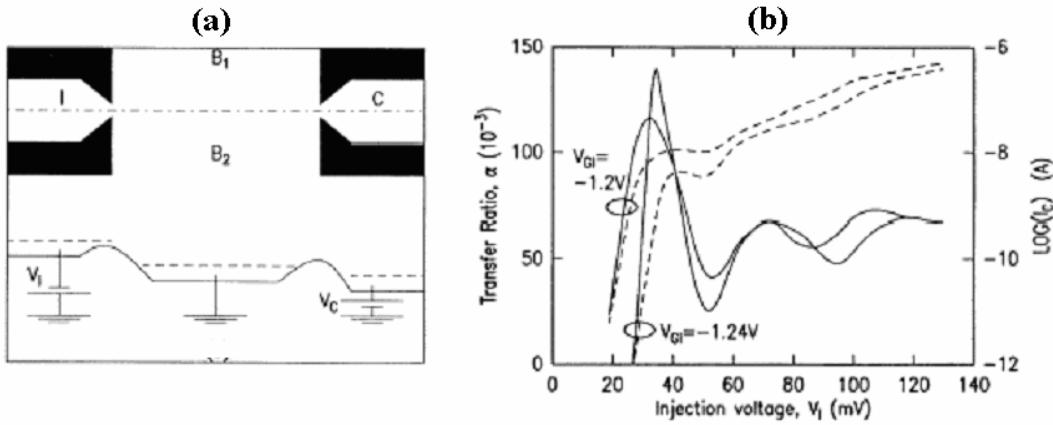
Figure 1.13 : Device that shows the long mean free path of hot electrons in 2DEG. (left) (a) Layout and energy diagram of structure. Dark regions are gates. I: Injector ; C: collector. (b) The oscillations in the transfer ratio (solid line) and collector current (dashed line) versus injection energy. At barrier energy is fixed to 23 eV above E_F. Two types of voltage for two values of injector gate voltages measured at T = 4.2 K. Noticeable negative differential transconductance (dI_C / dV_I). From U. Sivan *et al.* [13].
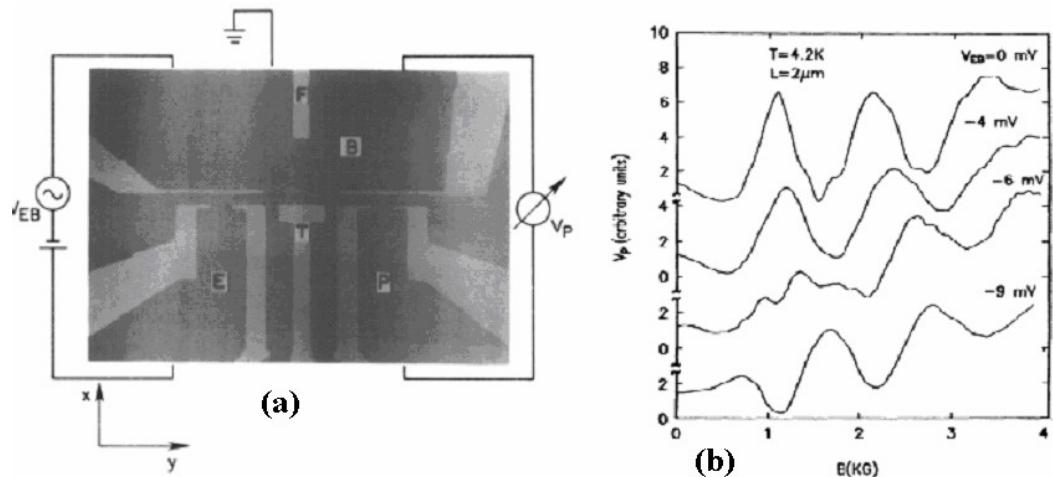
Figure 1.14: Device that shows the higher subband transition of hot electrons (a) Experimental Device (b) detected voltage versus magnetic field for different currents from B. Laikhtman, *et al.* [14].

1.5.3. Long Mean Free Path of Hot Electrons

Laikhtman *et al.* [14] tried to understand unexpected long free path results of Sivan *et al.* [13]. They suggested that the second subband transport can be the reason. Electrons with different injection energies are focused by magnetic field to a point contact (see Figure 1.14). Maximum potential of detector is shifted at -9 meV. Calculations from data showed the first-second subband energy difference is 15 meV. The result is also verified with Raman Spectroscopy. They concluded that long mean free path and the absence of electron-plasmon scattering (at about 10 meV) is due to higher subband transport.

1.6. Transport Effects Dominated by e-e Scattering

1.6.1. THETA Devices

Brill and Heiblum [38] fabricated a THETA (tunneling hot electron transfer amplifier). The structure is fabricated by molecular-beam epitaxy. They study the interactions of injected hot electrons and cold electrons, passing briefly through a thin doped GaAs. In this device, hot electrons are emitted by tunneling through very thin doped GaAs layer (see Figure 1.15.a). They observed electron multiplication at base region. Theoretical study of system shows that it is due to heating effect. High energy electrons increase the electron temperature in the base region which raises the current transfer ratio above unity. Directional scattering phenomenon is also discussed as a possible reason of electron multiplication. But magnetic field measurements agree with heating effect picture. As seen in Figure 1.15.c, transfer ratio exceeds unity when V_C (collector potential) is at positive bias. They have concluded that heating effect both depends on injection energy and current. Electron temperature is measured in the range of 10-20 K.

Dellow *et al.* [39] proposed that THETA device can be used to create THz oscillator, because e-e scattering is a very fast mechanism (10-100 fs).
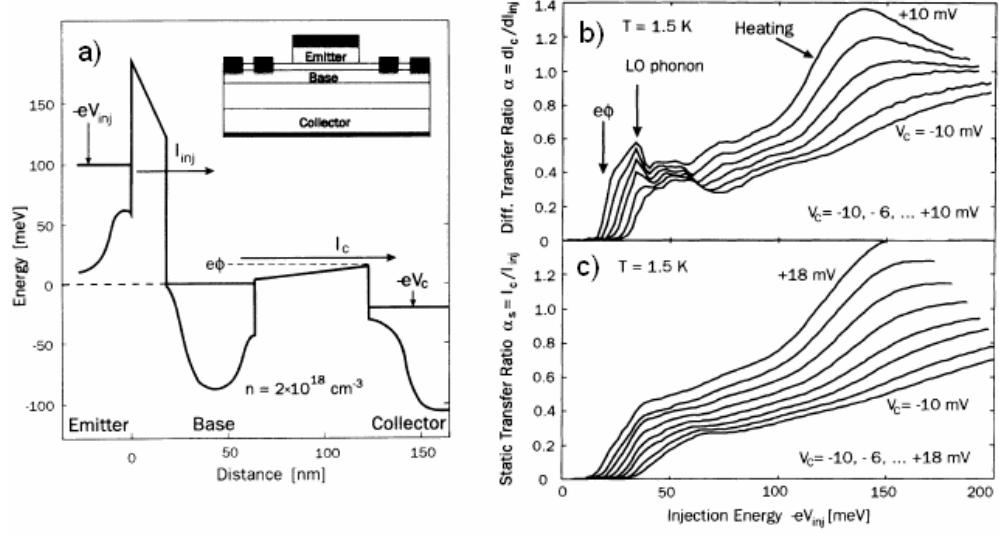
Figure 1.15 : THETA device ; (a) Conduction Band Profile of THETA device, with typical biasing, including band bending calculated from Poisson equation; (b) differential, (c) static transfer ratios, measured versus injection energy.

Kaya *et al.* [40] used in-stu focused ion beam implantation to fabricate hot electron transistor, similar to THETA device. Transfer ratio graeater than unity is observed. Schematic diagram of structure and negative resistance data are shown in Figure 1.16. and in Figure 1.17 respectively.
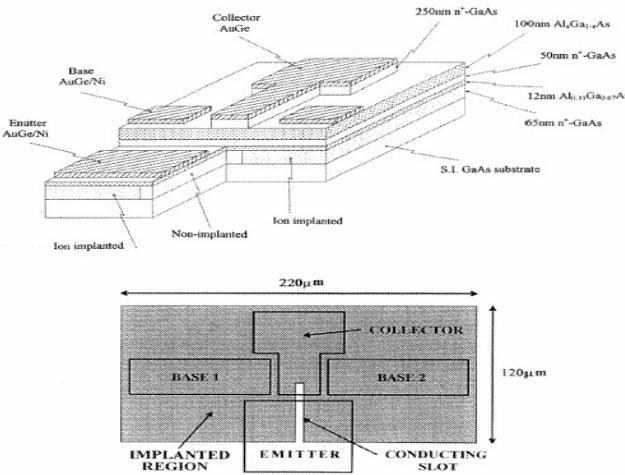
Figure 1.16 : Schematic diagram of oscillator structure (top) showing epilayer sequence, (bottom) vertical projection of completed structure.
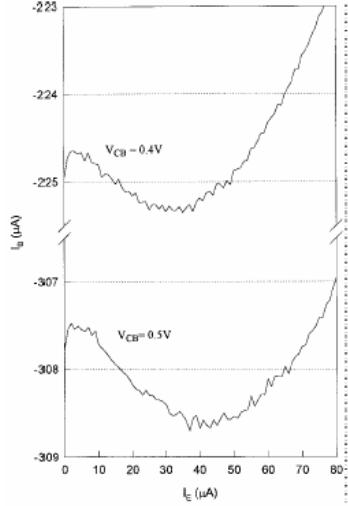
Figure 1.17: Base current as a function of emitter injection current at 2.4 K for V_{CB} = 0.4 and 0.5 V [40].

1.6.2. Absolute Negative Resistance in 2DEG:

Layout of the device is shown in Figure 1.18.a. [1]. This is a three terminal device, two electrostatic barriers are placed on asymmetrically patterned two dimensional electron gas. Electron multiplication effect results in a potential drop at the middle contact.   Momentum and current transfer ratio exceeds unity.   Negative resistance is attributed to directional electron-electron scattering.

In conventional electronic devices, electron transport is diffusive. The resistivity of these devices depend on electron impurity or electron phonon scattering. Electron-electron scattering does not effect the resistance of diffusive transport. But when the device dimension is smaller than impurity and phonon scattering, the transport is ballistic.

Electron-electron scattering is directional in two dimensional systems.   In general, electron-electron scattering is restricted to energy conservation, momentum conservation and Pauli's exclusion principle.   This restriction results small angle scattering in two dimensional systems.   Therefore when there is a hot electron, it is scattered with a cold electron without much loosing its direction.

Figure 1.18.c shows the base negative resistance that is measured.   There are three terminals in the device. Emitter (E), Collector (C) and base (B). The measurement of Figure 1.18, V_C and V_B are connected to ground. E is biased to -25 mV in order to

inject hot electrons. Therefore, electrons are injected from E and collected at B and C. Two electrostatic barriers are called gate emitter (V_{GE}) and gate collector (V_{GC}). V_{GE} is biased to -540 mV in Figure 1.18.c. Currents I_C , I_B and I_E is plotted versus V_{GC}. At low values of V_{GC} , injected current I_E is shared between collector and emitter. But at higher V_{GC} values (-270mV < V_{GC} < -350mV), I_B reverses its direction and I_E exceeds the value of I_C.
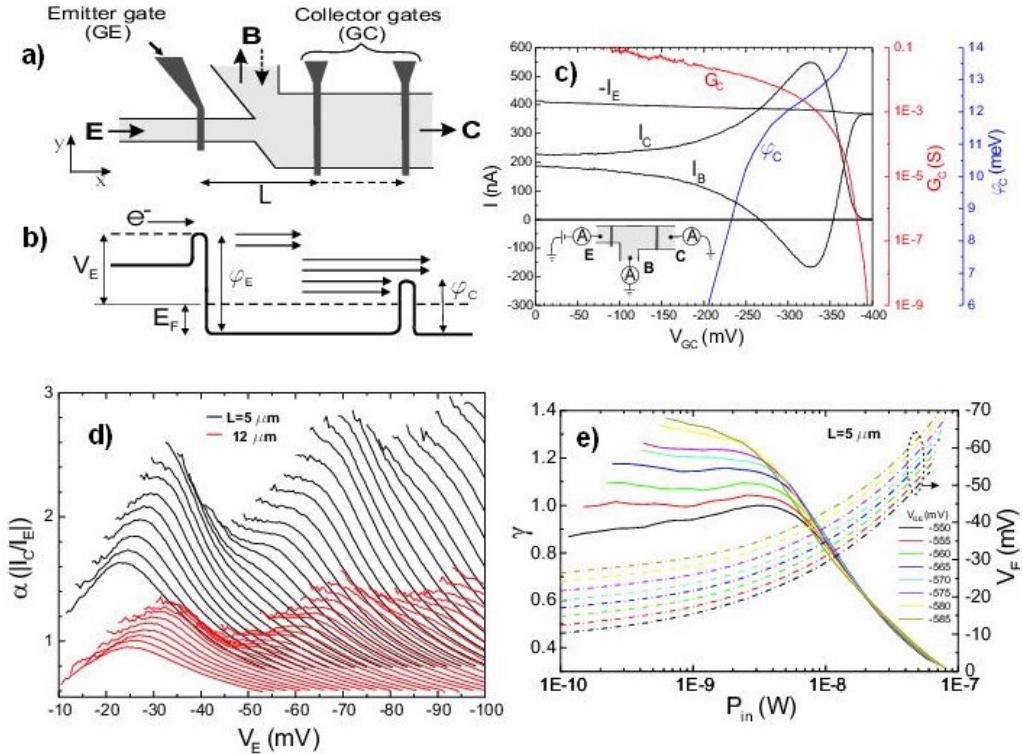
Figure 1.18 : The device that shows the absolute negative resistance in 2DEG from [1] (a) Layout of device, (b) Energy diagram of device, (c) Measured currents through three terminals, I_E, I_C and I_B versus collector gate voltage, V_{GC}; V_{GE} = -540mV, V_E = -25mV, $V_B = V_C = 0$. T = 4.2K, inset represents the measurement configuration. Curve labeled as G_C is the measured equilibrium conductance of the collector barrier for $V_C = 1mV$ (after substracting lead resistance), $V_{GE} = V_E = V_B = 0V$, f_C is the calculated collector barrier height from equilibrium conductance data according to Eq. 1.15. (d) The DC current transfer ratio a = | (I_C / I_E)| versus emitter voltage, V_E, as the emitter barrier is increased in steps, V_{GE} = -550mV,-555mV,.....-700mV, V_{GC} = -330 mV (e) The momentum transfer ratio, γ versus injected power calculated from data in (d) (solid lines) and corresponding V_E vs P_{in} curves (dashed line).

Electrons that are injected to E transfer their energy to cold electrons in the base region. Therefore, scatterred cold electron can also surmount collector gate barrier. Therefore, absolute negative resistance of base terminal is due to directional scattering. In directional scattering, momentum is preserved in one direction due to small angle between scattered electrons.

If, we assume the transmission probability of collector barrier as step function T (E$_-$) = T (E$_-$ - f_C). Then conductance can be calculated by

$$G_C = \frac{2ew\sqrt{2m^*}}{V h^2} \int_{\varphi_C}^{\infty} dE_X \int_0^{\infty} dE_y E_y^{-1/2} T(E_x) x \left[f_B(E_x, E_y) - f_c(E_x, E_y) \right] \qquad (1.15)$$

where w is the width of the collector channel, e is the charge of an electron. f_C and f_B are the distribution functions of base and collector terminal [1]. Dependence of f$_C$ on V$_{GC}$ can be calculated from Eq. 1.15. The resultant f$_C$ is shown in Figure 1.18.c.

Figure 1.18.d shows the injection energy dependence of transfer ratio | I$_C$ / I$_E$ |. With increasing injection energy, higher energy electron can surmount GE, hence scattered electrons will have higher momentum in order to surmount collector barrier. Therefore, transfer ratio increases with injection energy. The peaks at 36 meV and 72 meV are due to LO-phonon emissions. Dependence of transfer ratio on base length also agrees with directional scattering picture. At longer base lengths, electron-electron scattering broadening and impurity scattering will decrease the transfer ratio. It is seen in Figure 1.18.d.

In Figure 1.18.e, Momentum transfer ratio γ = (P$_{C,X}$ / P$_{E,X}$) versus injected power (P$_{in}$) is plotted. P$_{E,X}$ and P$_{C,X}$ is given as;

$$P_{E,x} = \sqrt{2 m^* e (V_E + E_F)} I_E / e \qquad (1.16)$$

$$P_{c,x} = \sqrt{2 m^* \varphi_C} I_C / e \qquad (1.17)$$

where e is equal to one electron charge, m* is reduced mass of electron, E$_F$ is the fermi energy, f_C is the height of collector barrier.

Also in Figure 1.18.e, V$_E$ versus P$_{in}$ is plotted. P$_{C,X}$ and P$_{E,X}$ are calculated from V$_E$ values, and collector barrier height. Interestingly, momentum transfer ratio is also exceeding unity in some curves. Therefore, in one direction, momentum of collected electrons is greater than that of injected electrons.
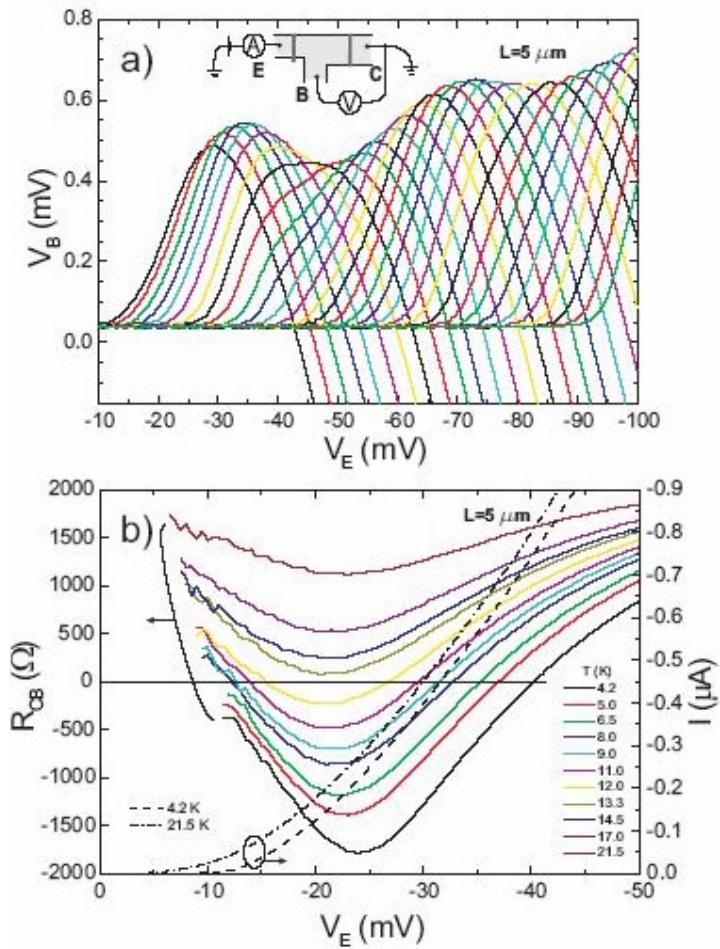
Figure 1.19 : Measured base potential and absolute negative resistance of device from [1] (a) Base Voltage, V_B versus V_E for the same set of V_{GE}, V_{GC} values as in Figure 1.18.d. Inset shows the measurement configuration (b) Three terminal resistance; $R_{CB} = (V_B - V_C) / I$ and current, $I = I_E = -I_C$ versus V_E at various temperatures. $V_{GE} = -550$mV, $V_{GC} = -340$mV.

In Figure 1.20.a base terminal potential is measured with respect to collector terminal when I_B equals to zero. V_B versus V_E is shown in the figure. When I_B smaller than zero in current measurements, V_B is higher than zero in the voltage measurements. Figure 1.20.b shows the calculated base terminal resistance at different temperatures. As seen in the figure, absolute negative resistance of base terminal decreases with increasing temperature.

1.6.3. Quantum Electron Pumping

Govorov and Heremans [41] theoretically studied hydrodynamic phenomena originating from electron-electron collisions in two dimensional Fermi system. Theoretically, they offered that electron beam sweeping past an aperture creates a pumping effect. They proposed that main reason of this phenomenon is specific potential distribution induced by the injected electrons. Therefore, repulsive coulomb interaction between electrons would form attractive force when passing from an aperture. They have characterized system theoretically and proposed that this pumping effect is qualitatively different from Bernoulli pumping effect. Figure 1.20.a shows the pumping effect schematically. Inset shows the theoretical dependence of pumping effect on temperature. Figure 1.20.b shows the nonequlibrium electron density as a function of the in-plane coordinates. As seen in Figure 1.20.b, nonequlibrium electron density has high positive value at the middle but in the neighbor region, nonequlibrium electron density has negative values. This is atributed to form pumping effect.
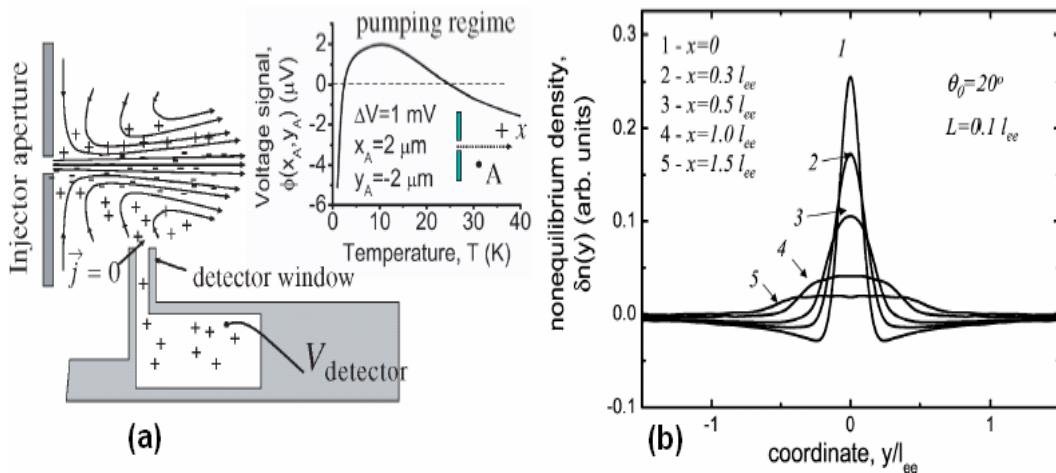
Figure 1.20 : Theoretical quantum electron pumping device from [41] : (a) Schematic of theoretically offered quantum electron pumping in theoretical mesoscopic device. (b) Calculated nonequilibrium electron density as a function of in-plane coordinates. l_{ee} = e-e scattering mean free path.

Chapter 2

EXPERIMENT

In the experimental part the fabrication procedure and measurement setup is described. Then, mechanism of electron multiplication is shown. Lastly, characterization of device is explained.

2.1 Fabrication:

2.1.1. Cleaving and Cleaning

- Sample is cleaved 5 mm X 5 mm dimensions.
- Wafers are cleaned in ultrasonic cleaner in the acetone for 5 minutes.
- Wafers are cleaned with 3 steps of Aceton and 3 steps of IPA.
- Samples are dried with gas N_2.
- Dehydration at 110 ^{o}C for 1 minute.

2.1.2. Mesa

- Spin of AZ-5214 with 6000 rpm for 40 second.
- Bake on hot plate at 110°C for 50 second.
- Expose UV light for 40 second with at 5 mW / cm^2 with Mask- LEP-M.
- Develop with 1:4 AZ-400 K**:**H_2O for 20 second
- Post-bake: 110°C for 2 minutes.

- Etch in 1:H_2SO_4+8:H_2O_2+320:H_2O for 45 second.
- Dektak measurements show the depth of 100 nm.
- Clean with Aceton + IPA + Dry N_2.

2.1.3. Ohmic Contacts

- Clean with Aceton + IPA + Dry N_2.
- Spin: 1300 rpm / 2 second ; 6000 rpm / 40 second.
- Bake at 110°C for 60 second.
- Exposure with Mask-LEN at 6 mW/cm^2 for 9 second.
- Postbake on hotplate at 120°C for 2 minutes.
- Flood exposure (no mask) at 6 mW/cm^2 for 28 second.
- Development with AZ-726 K for 55 second.
- Box Coater Evaporation: 350 Å Ge + 700 Å + 400 Å Ni + 1500 Å Au.
- Lift-off with Aceton for 2 hours.
- Anneal in forming gas at 450°C for 60 second.

2.1.4. Fine Gates with Electron Beam Lithography

- Clean with Aceton + IPA + Dry N_2.
- Spin with 1000 rpm for 4 second + 4000 rpm for 60 second which gives 140 nm resist thickness.
- Bake in oven at 160°C for 1 hour.
- E-beam pattern is drawn on resist with e-beam system with dose: 260 μC / cm^2.
- Develop in 1:3 MBIK:IPA for 60 second, rinse in IPA 60 second, Dry with nitrogen gas.
- Box Coater Evaporation: 50 Å Cr + 150 Å Au.
- Lift-off with Aceton for 12 hours.

2.1.5. Gate Pads

- Clean with Aceton + IPA + Dry N_2.
- Spin Az-5214, 1300 rpm / 2 second , 6000 rpm / 40 second.

- Bake on hot plate at 110°C / 60 second.

- Exposure using Mask-LEN-G at 6 mW / cm^2 for 9 second.

- Postbake on hotplate at 120°C for 2 minutes.

- Flood exposure at 6 mW/cm^2 for 28 seconds.

- Develop in AZ-726 for 55 second.

- Box Coater Evaporation 100 Å Cr + 1500 Å Au.

- Lift-off with Aceton for 12 hours.

2.1.6.Bonding

- Devices are cleaved into individual devices.
- Each device is attached to chip holder with AZ-5214 resist.
- The pads are connected by wire bonding.

2.2. Device:
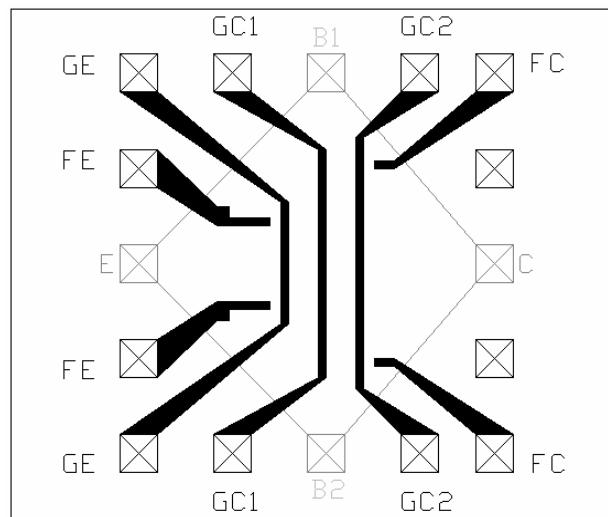
Figure 2.1 : Schematic of Device that is fabricated: Ohmic Contacts: (E: Emitter; C: Collector; B1: Base1; B2: Base2); Metallic Gates: (FE: Focus Emitter; FC: Focus Collector; GE: Gate Emitter; GC1:Gate Collector1; GC2: Gate Collector2). The diamond shape is the mesa. The drawing is not to scale.

A new developed device schematic is shown in Figure 2.1. The distance between GE barrier and GC1 barrier is 1 µm. The distance between GE barrier and GC2 barrier is 2 µm. Focus peaks to gate is 300 nm. Gates are used to isolate the barrier region (e-beam paterned region) from the rest of the device.

In the developed fabrication procedure, FE and FC are used in order to define conductor. In this way one can reduce the device size to submicron. Previous design was using etched mesa and gates. Alligning of mesa to gates were not easy. In the new scheme, we define the conductor by FE and FC and hence there is only one EBL step.

Optical lithography had three layers, first layer was mesa layer, second was ohmic contact layer, third was called gate layer. Mesa layer is used to etch the 2DEG layer, so that we fabricate a shaped 2DEG layer. Second layer was ohmic contact which is used to send and receive electrons to 2DEG active layer. Third layer is gate, which is used to form barriers and focus on 2DEG. The actice device is placed at the center.

Gate metals are made by Cr/Au evaporation. Chromium is used to stick the metallic layer to 2DEG wafer surface, because Au can not stick to the surface of 2DEG. After Cr, we coat Au on Cr, because Au is very good conductor and very resistive against to oxidation. In the development process of this method. In the initial devices Ti is used instead of Cr. However, conduction is observed between optic lithography and ebeam lithography, possibly due to the oxidation of Ti.
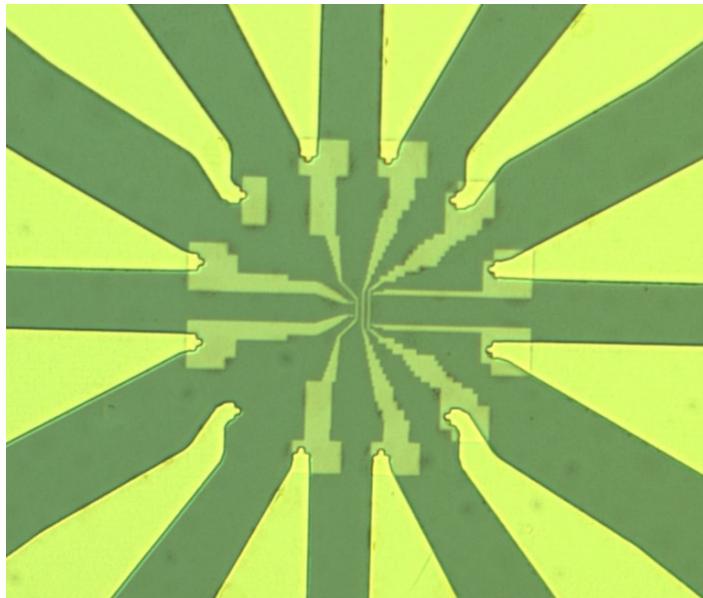
Figure 2.2 : Photograph of the fabricated device taken by an optical microscope.
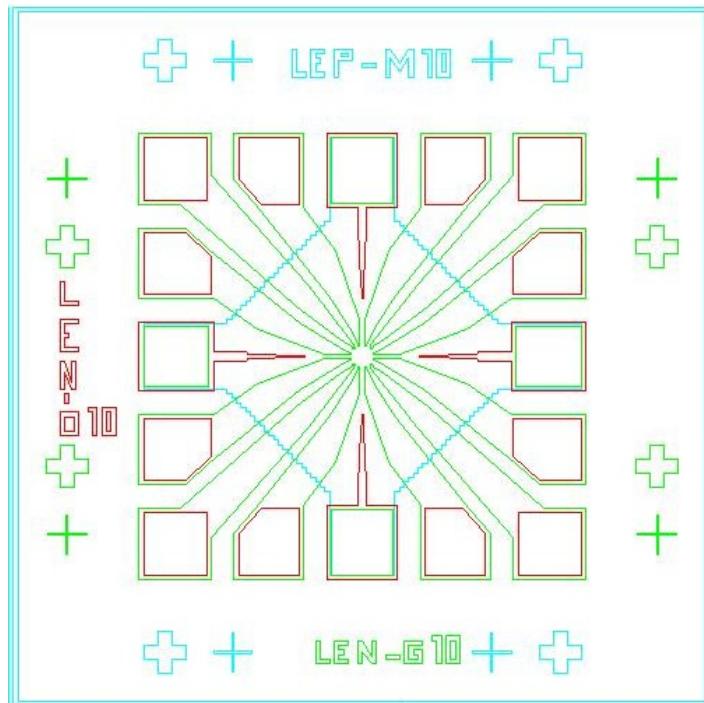
Figure 2.3: AutoCAD Drawing of optical lithographic layout. Red is the ohmic contact, blue is the mesa layer, green is metallic gates.
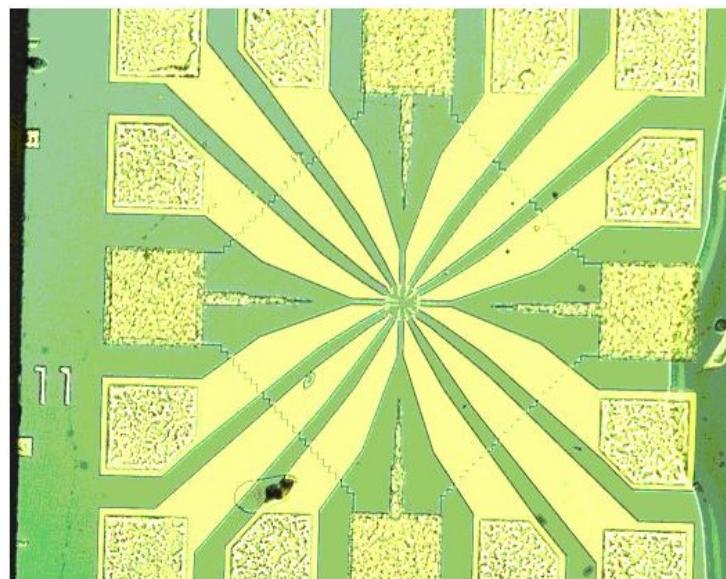
Figure 2.4: Optical microscopy of fabricated device.

Metallic gates on surface of the 2DEG are used to deplete the 2DEG electrostatically. Biasing a negative potential on the gates decreases the electronic

density under it and forms a barrier. This property of 2DEG is used in barrier regions of the device. If high enough negative bias is given to the gates, they totally deplete the electron density under them and they inhibit the electron transport. This property is used in the focus gates. By applying high negative bias (-1,9 V) to FE and FC, the conducting area gets into the pattern defined by gates.

Working principles are similar to previous design [1] which is explained in section 1.6.3. Directional scattering and electron multiplication is explained in section 2.3. Schematics of the our device is shown Figure 2.1. Energy diagram of the device can be seen in Figure 2.6. There are two types of gates in the design (focus gates and barrier gates). Electrostatic focus gates are used to define the conductor. With high bias of focus gates, two dimensional channel is formed instead of etched conductor of previous design. GE and GC2, are used to form electrostatic barriers. GE is used to inject hot electron to base region as seen in Figure 2.6. GC2 is used to collect scattered electron beam. If we don't use, GC2, scattered electrons will thermalize and we could not see electron multiplication. Ohmic contacts E, B1, B2 and C are used to inject and collect the current.

In the development process of this fabrication method, positive AZ5214 (see Figure 2.5.b) is used which results lift-off problems of gates and ohmic contact. Finally, negative AZ-5214 is used in the process (see Figure 2.5.a), which solves the lift-off problem.

(a)   (b)
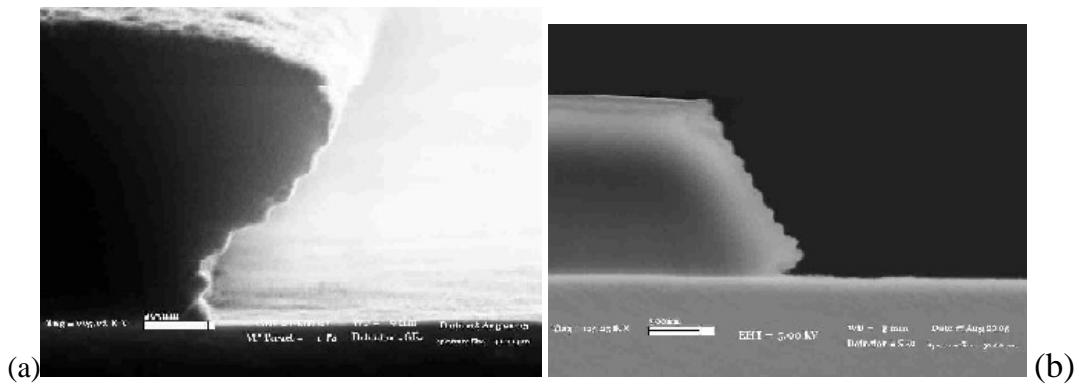
Figure 2.5 : SEM image of positive and negative profile of AZ-5214 (a) Negative AZ-5214 profile after development, (b) Positive AZ-5214 profile after development.

2.3. Mechanism
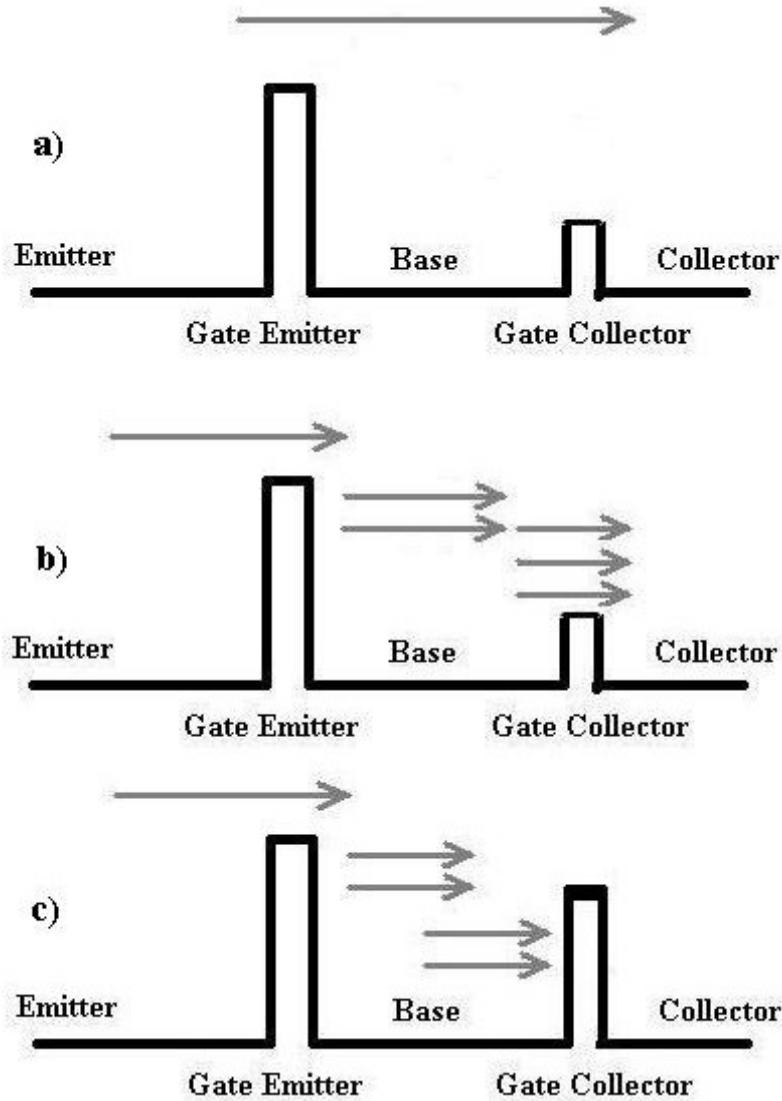
Figure 2.6 : e-e scattering mechanism in the device; In (a), (b) and (c), it is assumed that base length is smaller than mean free path of electron, therefore, system is ballistic. (a) when all emitter current pass the base ballistically, not electron multiplication, (b) e-e scattering results electron multiplication; (c) e-e scattering can not result electron multiplication due to high collector barrier.

In Ref. [2] it has been shown that electron-electron scattering results in negative resistance. The mechanism that is proposed in there is shown in Figure 2.6. If injected electrons surmount GE, they transfer their energy to cold electron. Energy transfer occurs via electron-electron scattering. When a hot electron is scattered by cold

electron, a multiplied beam of electron are formed. In 2DEG, electron-electron scattering is small angle process [21]. Therefore, multiplied electrons convey their forward momentum for several generations. If beam of electrons can surmount collector barrier, electron multiplication due to directional scattering is observed.

2.4. The Measurement Setup

The measurements are done at 4.2 K with Agilent 4156C Precision Semiconductor Parameter analyzer. Sample is inserted into the liquid helium transportation dewar with a temperature sensor on it.

1.5 K measurements are done with Oxford Instruments Cryostat. 1.5 K temperature is reached with pumping the liquid helium in the sample space by a rotary pump. Cryostat has a Superconducting Magnet that has been used to test the effect of magnetic field. Temperature measurements are done by Oxford Instruments ITC 503 temperature controller.

1.5 K measurements are done after the initial tests at 4.2 K measurement. 4.2 K measurements showed the base terminal current reversal as expected [1]. However, unexpected collector terminal terminal current reversal is also observed. The aim of 1.5 K measurements is to investigate further this affects. Variable temperature and magnetic field are the other parameters which we used in 1.5 K measurements.
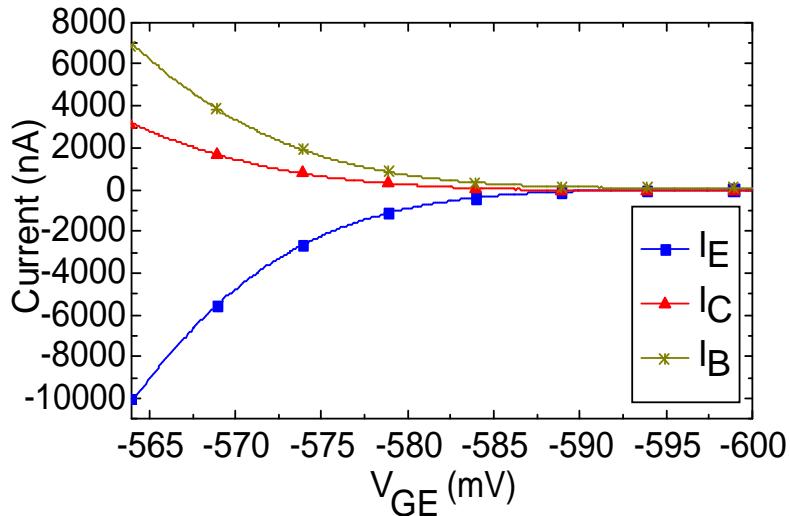
Figure 2.7: Testing of emitter gate function, I_E , I_C and I_B versus V_{GE}; V_E = -100mV; V_F = 0; V_B = V_C = 0. 1mV

2.5. Device Characterization
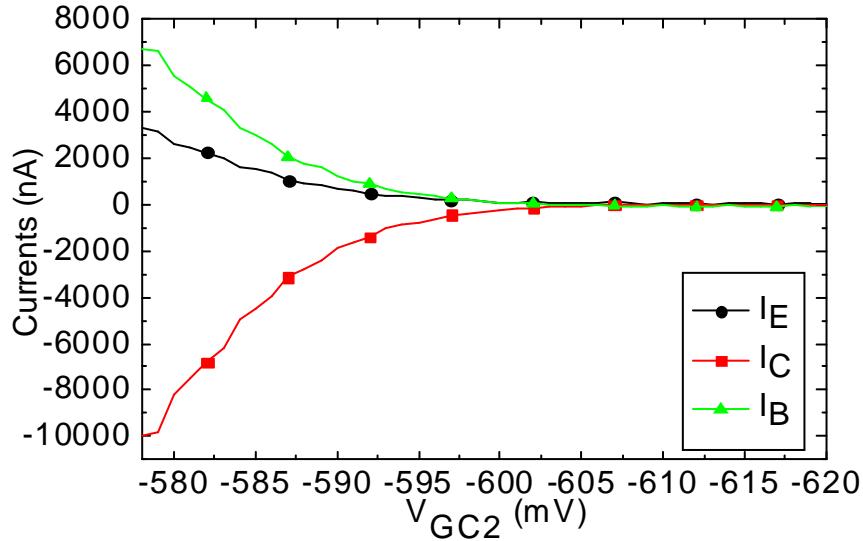
Figure 2.8 : Testing of GC, I_E, I_C and I_B vs V_{GC2}; $V_C = -100mV$; $V_F = 0V$; $V_E = V_B = 0V$.
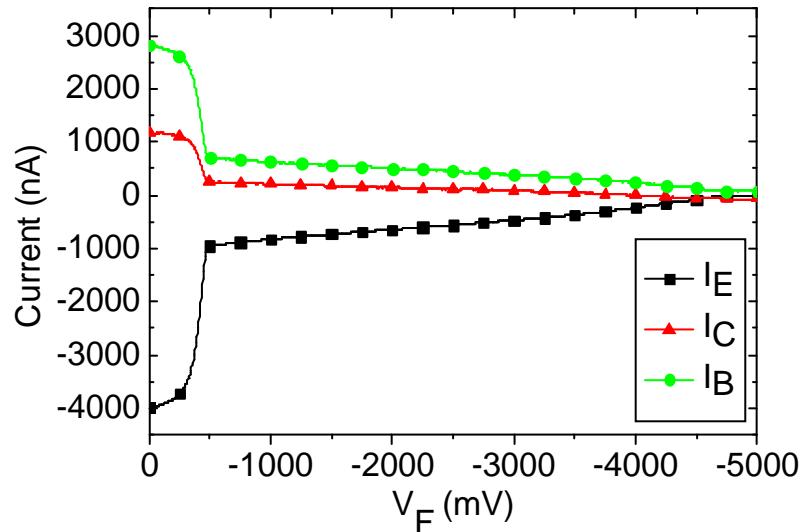
Figure 2.9 : Testing of FC. Currents through the terminals vs V_F, $V_E = -1$ mV, $V_E = V_B = 0$ V.

Characterization of the device is started with testing of the barriers. This test is important to verify that gates can deplete the 2DEG completely. If a gate can not deplete the 2DEG layer, then current may leak on the undesired paths.

Figure 2.7 shows the testing of GE. At the values of 595 mV, I_E becomes zero; verifying that the gate emitter works.

FE can also block all electrons under the focus gates at about -600 mV (see Figure 2.9). This shows that at -600 mV, electrons can only transport through the opening defined by FE. Further increasing the bias from -600 mV to -5 V depletes opening and current is reduced to zero.

Figure 2.8. shows that the FC can also block all electrons at -605 mV.

Chapter 3

RESULTS AND DISCUSSION

Data is collected at 4.2 K and 1.5 K with 4156C Semiconductor Analyzer. Ohmic contacts (E, C, B1 and B2) are used to inject carriers to 2DEG active layer. Focus gates (FC and FE) are used to form narrow electrostatic transport channel. In Ref. [1] the device has an etched 2DEG channel. The channel has a width of 2 µm. There is no narrow mesa channel in our device. Similar narrow channel is formed by focus metallic gates. Isolation is obtained by negative biasing of FE and FC that are connected together in all measurements. At 4.2 K, $V_F = -1.9$ V is applied. Later, at 1.5 K, $V_F = -2.2$ V is used. Bias is increased in 1.5 K measurement, because some leakage current in 4.2 K measurement is observed. Increasing the bias to -2.2 V at 1.5 K measurements have solved the leakage current problem.

In Ref. [1] the device had only one base terminal, whereas the device in this study has two base terminals B1 and B2 which are connected to each other in the measurements. This is expected to increase the base negative voltage and current.

In Ref. [1] the device had two different gate barriers (12 µm and 5 µm). Our device has also two gate barriers. GC1 is 1 µm away from GE. GC2 is 2 µm away from GE. While designing the device, the idea was to make measurement with both GC1 and GC2. In measurements, absolute negative resistance with GC2 is observed. However, the same effect with GC1 is not observed. The reason can be the electrostatic channel that is formed between GC2 and FC. This electrostatic channel cannot be formed between GC1 and FC, because the distance between them is very high. This distance is 300 nm between focus collector and GC2, but 1.3 µm between focus collector and GC1.

Focus gate at 2.2 V bias can form electrostatic channel to GC2, but it can not form electrostatic channel even at -7 V bias to GC1. Without electrostatically isolated channels, leakage current from other sides of the device destroys the directional scattering effect.

The device is designed in order to observe the absolute negative resistance at the base terminal. However, in the measurements absolute negative resistance at collector terminal is also observed.

3.1. 4.2 K Measurements

All measurements are started at the temperature of liquid helium, 4.2 K. The device is mounted on to the socket in the sample holder. The sample holder is dipped into the liquid helium dewar. The measurements are done with 4156C Semiconductor Analyzer.

After observing proper device operation, the measurements are performed at 1.5 K. The reason for the experiments to be taken 1.5 K, is to further reduce the phonons in 2DEG and to increase the mfp of electrons.

In order to observe all related phenomena about absolute negative resistance, and because of nine independent variables that neede to be varied, a strategic plan for measurements is needed. These variables are the voltages on FC (V_{FC}), FE (V_{FE}), Base1 (V_{B1}), Base2 (V_{B2}), Emitter (V_E), Collector (V_C), Gate-Collector1 (V_{GC1}), Gate-Collector2 (V_{GC2}) and Gate-Emitter (V_{GE}). In order to make reasonable number of measurements, some parameters have to be taken as constants. Thus, FC and FE are biased to a constant value. At 4.2 K, bias was 1.9 V. Furthermore, absolute negative resistance can not be observed with GC1 due to the reasons that mentioned before. As a result, the measurements have 5 independent variables; V_E, V_C, V_B, V_{GE} and V_{GC}.

3.1.1   Dependence of Currents on Injection Energy.

I_E, I_B, I_C is measured with respect to V_E for various V_{GC} and V_{GE} settings. Current reversal at the base terminal is an expected phenomenon [1]. Negative I_B (Figure 3.1) is observed at specific values of V_{GC}, V_{GE} and V_E, this is due to mechanism of electron multiplication (See Figure.2.6). I_B has a minimum value of -210 nA at injection energy of -225 mV, at V_{GE} = -750 mV and V_{GC2} = -390 mV.
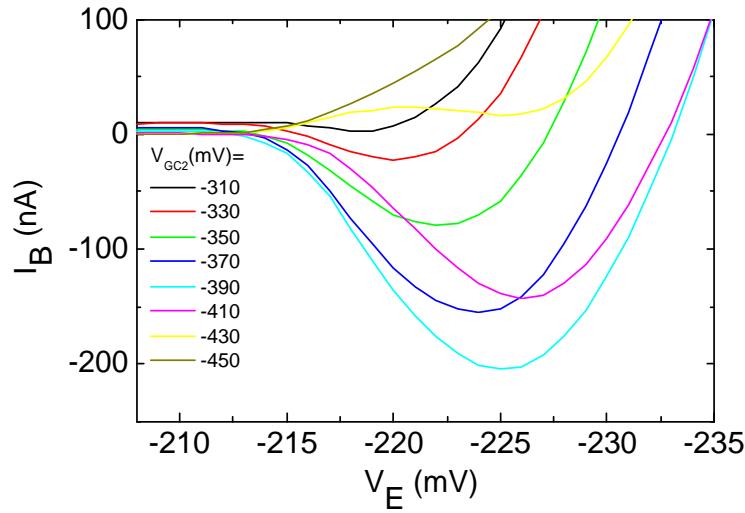
Figure 3.1 : I_B versus V_E at different V_{GC2} values at 4.2 K. V_{GC2} = -310, -330,.....-450 mV; V_{GE} = -750 mV, V_B = V_C = 0 V.
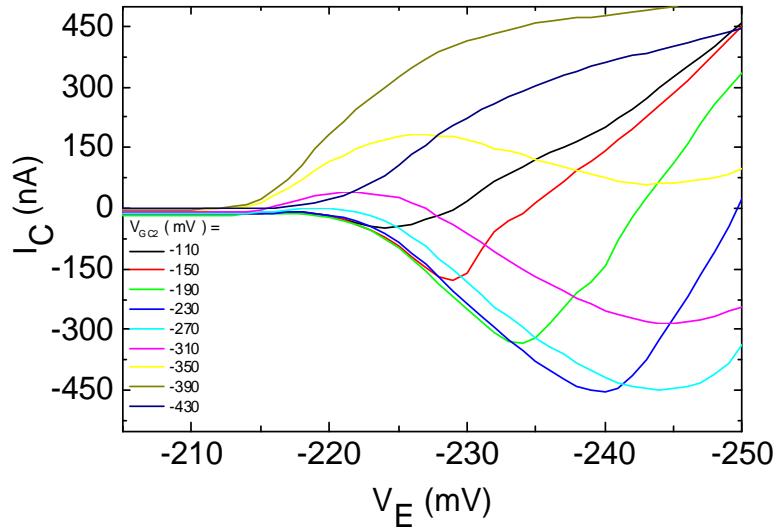
Figure 3.2 : I_C versus V_E at various V_{GC2} values at 4.2 K. V_{GC2} = -110, -150.....-430 mV; V_{GE} = -750 mV.

Current reversal at the collector terminal is an unexpected phenomenon. Negative I_C (Figure 3.2) is observed at different specific values of V_{GC}, V_{GE} and V_E in comparison to negative I_B (Figure 3.2). At the same V_{GE}, negative I_C is observed at higher injection energies. Despite that, I_C is observed at lower values of V_{GC2}. This can

be related to heating effect of base region [30] (see Figure 3.7). I_C has minimum value of -450 nA at specific V_{GE}, V_E and V_{GC2} as shown in Figure 3.2.

3.1.2   Dependence of Base Current on the Emitter Barrier

Base current reversal is further investigated in this section as a function of V_{GE}. Results are shown in Figure 3.3 and Figure 3.4. With increasing V_{GE}, injected electrons need higher energies to pass the barrier. Higher energy electrons have lower mean free path [3]. Lower mean free path results higher number of electron-electron collisions in the base region (see figure 2.6). There is higher negative current in the base terminal with increasing V_{GE} as shown in Figure 3.4.

Figure 3.3 is the original experimental data. As seen in the data, there is some leakage current from collector to base. V_F is not enough to close the distance between GC2 and FC. The problem is solved by increasing the bias from -1.9V to -2.2V in 1.5 K measurements.
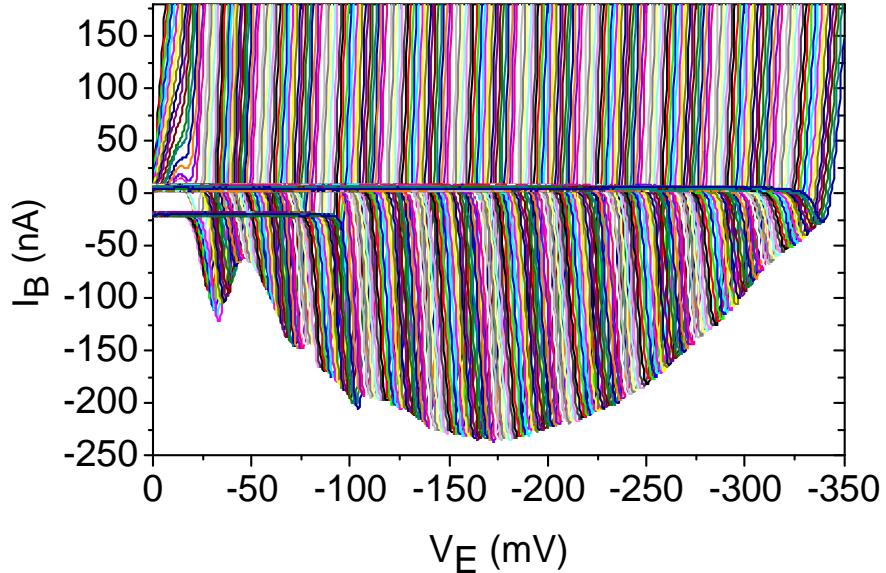
Figure 3.3 : I_B vs V_E at various V_{GE} values at 4.2 K. V_{GC2} = -390 mV; V_{GE} = -400mV to -920mV in 2mV steps; $V_B = V_C = 0$.

There are four peaks in the data of Figure 3.4. As discussed previously, negative resistance of base terminal increases with increasing V_{GE}, but it has some limit.

If electron energy exceeds 36 mV, then an optical phonon is emitted with the energy of 36 mV reducing the energy of electron. Three peaks in the graph that are at 36mV, 72 mV and 108 mV corresponding to one two and three longitudinal optical phonons (LO-phonons) of GaAs strcture. The monotonic decrease higher than -170 mV of V_E, is attributed to heating of the electron system.
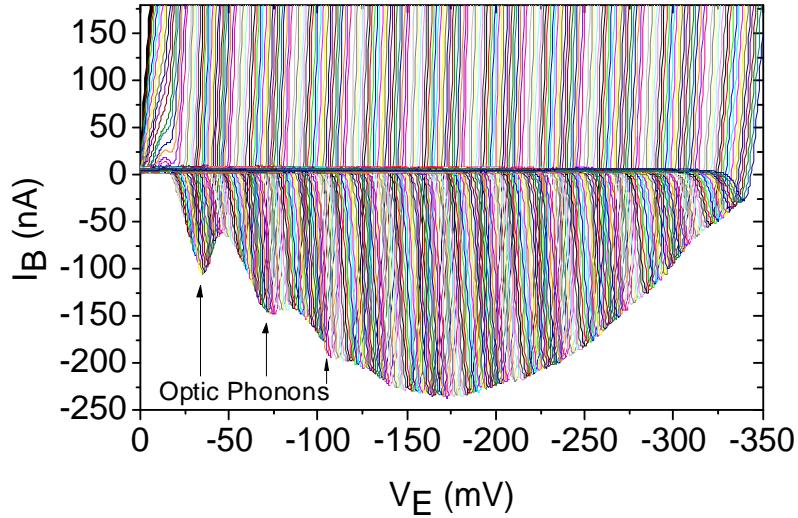
Figure 3.4 : Same curves as in Figure 3.3 after subtracting the leakage currents.

3.1.3   Dependence of Collector Current on the Emitter Barrier

Negative collector current at various collector barrier height is seen in Figure 3.5. Figure 3.6 is after correcting the leakage current. There is only one peak in the data of Figure 3.6.   Increase of negative collector voltage up to -260 mV is due to effect of heating. In higher injection energies, negative potential decrease. This decrease is due to heating of collector terminal.

Negative I_C has minimum value of -500 nA. The mechanism of collector current reversal is possibly not directional scattering. Instead, negative I_C is the result of heating of base region. High energy electrons heat the base region. Heating will reduce the chemical potential in two dimensional systems [42]. Chemical potential decrease in base region will result in potential gradient between base and collector. Therefore, if GC is low enough, electrons flows from collector to base region. (see Figure 3.7)
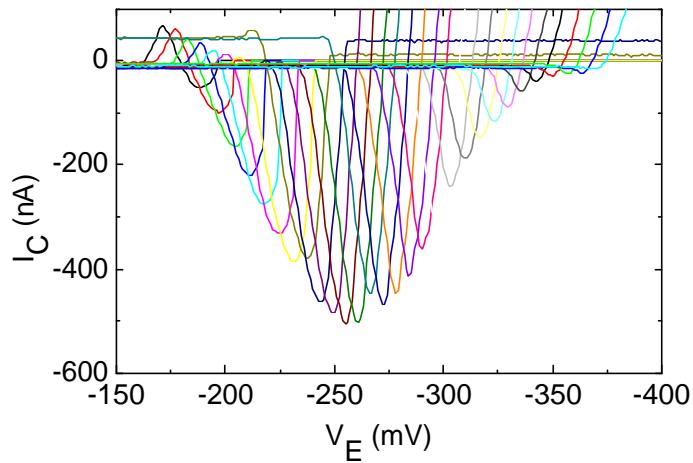
Figure 3.5: I_C vs V_E at various V_{GE} values at 4.2 K, $V_F = -1,9V$; $V_{GC2} = -250mV$; $V_{GE} = -670mV$ to $-950mV$ with $-10mV$ steps; $V_B = V_C = 0$ V; $V_F = -1.9$ V.
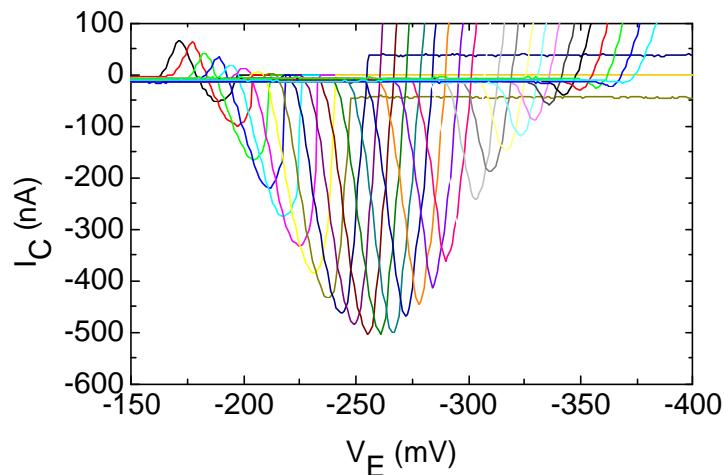
Figure 3.6 : Data in Figure 3.5 after leakage current corrections.
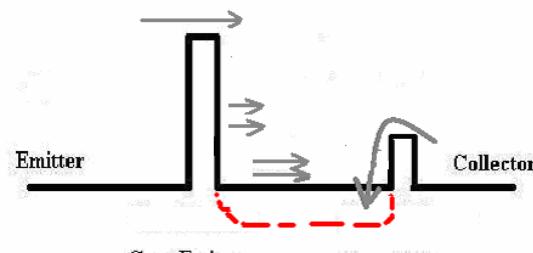
Base Heating of 2D system
2D Systems: Chemical Potential decreases with Heating

Figure 3.7 :   Collector current reversal due to Base Heating at high Emitter Current.

3.1.4 Dependence of Currents on Collector Barrier at Different Emitter Barrier Heights

Previous measurements showed us that collector barrier height is both critical in the mechanisms of negative resistance of base and collector. Therefore, we measured the dependence of currents on collector barrier height at different emitter gate heights. Figure 3.8 shows the dependence of I_B on V_{GE}. Figure 3.9 shows the collector current dependence on collector barrier height. At small values of V_{GC2}, I_B is constant. Then with increasing collector barrier I_C increases. This increase is reasonable, because with increasing collector barrier height, collector resistance increases. Therefore, electrons prefer to go base terminal. Further increase of V_{GC2} results in decrease of I_B. This decrease is due to directional scattering. Scattered electrons directly pass to collector region. (see Figure 2.6.b)
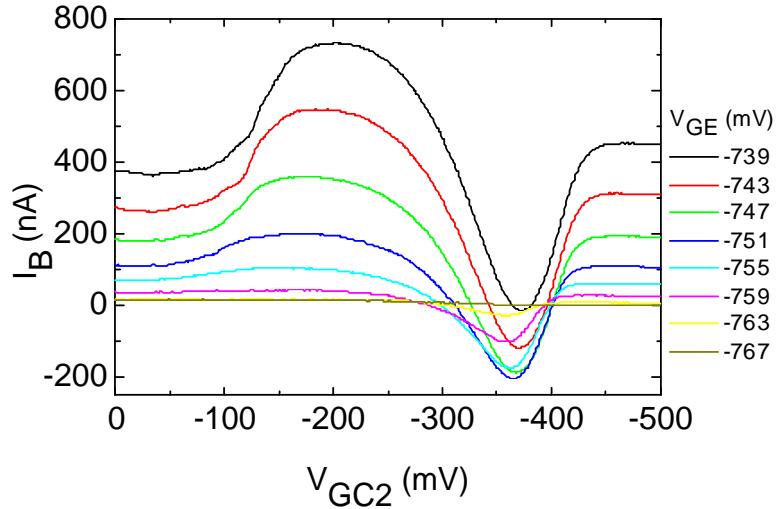
Figure 3.8: I_B versus V_{GC2} at various V_{GE} values at 4.2 K. ; V_{GE} = -739 mV, -743 mV, -747 mV, -751 mV, ..., 767 mV; V_E = -226 mV; V_B = V_C = 0 V; V_F = -1.9 V.

I_C and its dependence on GC height is shown in Figure 3.9. There are four different regions. At small values of V_{GC2}, I_C is not dependent on V_{GC2}. Because V_{GC2} does not deplete the active layer at small values. Between -100 mV to -200 mV, there is a decrease of current down to -300 nA. Decrease to a negative value is due to heating

effect (see Figure 3.7). Further increase of negative biasing of V_{GC2} results an increase of I_C up to 600 nA. As seen in Figure 3.9.b, transfer ratio $| (I_C / I_E) |$ exceeds unity at when V_{GC2} equals to -370 mV and V_{GE} equals to -740 mV. Therefore, there is directional scattering. We can see both directional scattering and heating effect in the same graph at the same injection energy. This is an interasting border between two competing phenomenon. (see section 2.4). In the interval from -390 mV to -500 mV, GC2's height starts to inhibit electron multiplication and I_C decreases to zero.
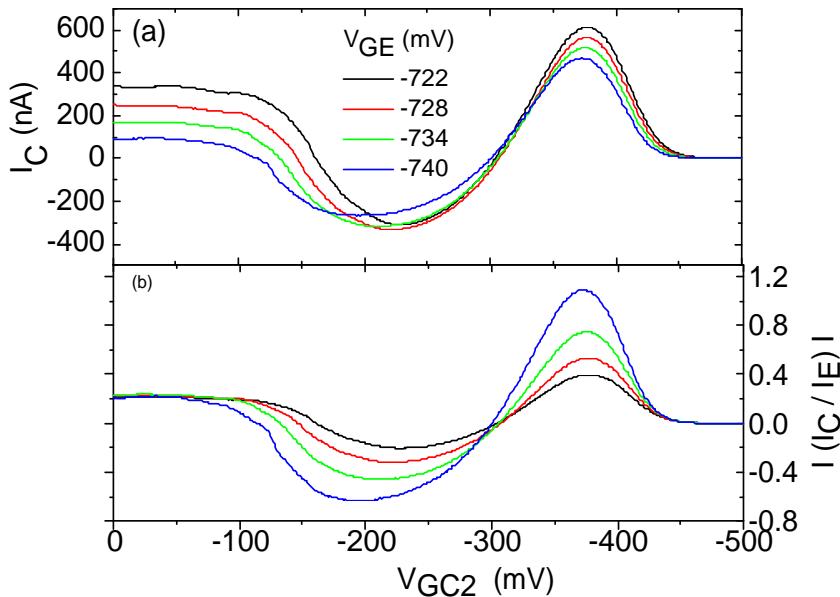
Figure 3.9: I_C versus V_{GC2} various V_{GE} values at 4.2 K and transfer ratio; (a) V_{GE} = -722 mV, -728 mV, -734 mV, -740 mV; V_E = -226 mV. (b) Transfer ratio $| (I_C / I_E) |$ calculated from a.

3.1.5 Dependence of Base Terminal Potential on Injection Energy

In previous measurements, electron multiplication is observed by current recording. In this measurement, we make $I_B = 0$ A and we only measure V_B with respect to V_C. Figure 3.10 shows the resultant V_B. This is the result of electron multiplication effect [1]. In this configuration, electron multiplication results in a maximum of 2 mV potential at -230 mV injection energy.

3.1.6 Dependence of Collector Terminal Potential on Injection Energy

In this measurement, we measure V_C at $I_C = 0$ A to observe the effect of base heating (see Figure 3.7). Figure 3.11 shows the result. Measured V_C has a maximum of 1 mV at -270 mV. Absolute potential is lower compared to base potential due to directional scattering. This result shows experimentally that heating base region results in a positive potential in collector terminal. Also, in agreement with the current measurements, the collector positive potential is observed, if the height of GC2 is low.
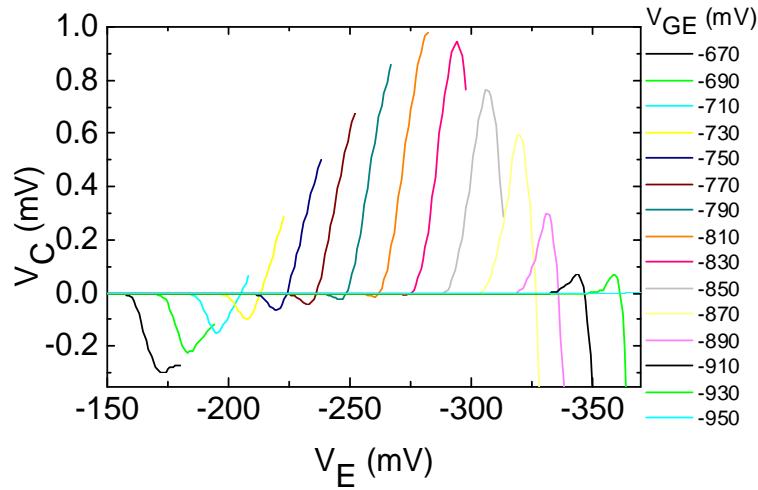
Figure 3.10: V_B versus V_E at various V_{GE} values at 4.2 K ; V_{GE} = -670 mV, -690 mV ,...., -950 mV; V_F = -1.9 V; I_B = 0 A ; V_C = 0V ; V_{GC2} = -370 mV.

3.1.7 Current Transfer Ratio

Electron multiplication mechanism can result in negative current and positive potential at the base terminal in various configurations. Transfer ratio (a = $|I_C / I_E|$) is the ratio of collected electron at collector over emitter electron from emitter terminal (Figure 3.12). Transfer ratio increases with injection energy. This is reasonable; because with increasing energy, electron's mean free path decreases. Therefore, number of electron-electron scattering events increases in the base region, which increases the transfer ratio.
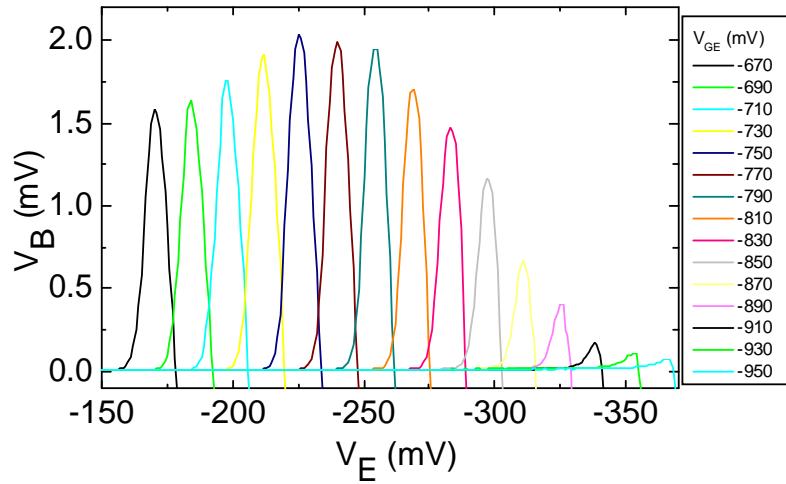
Figure 3.11 : V_C versus V_E at various V_{GE} values at 4.2 K; V_{GE} = -670 mV, -690 mV, -710 mV,..., -950 mV; V_F = -1.9 V; V_{GC2} = -260mV; I_C = 0 A; V_B = 0 V;
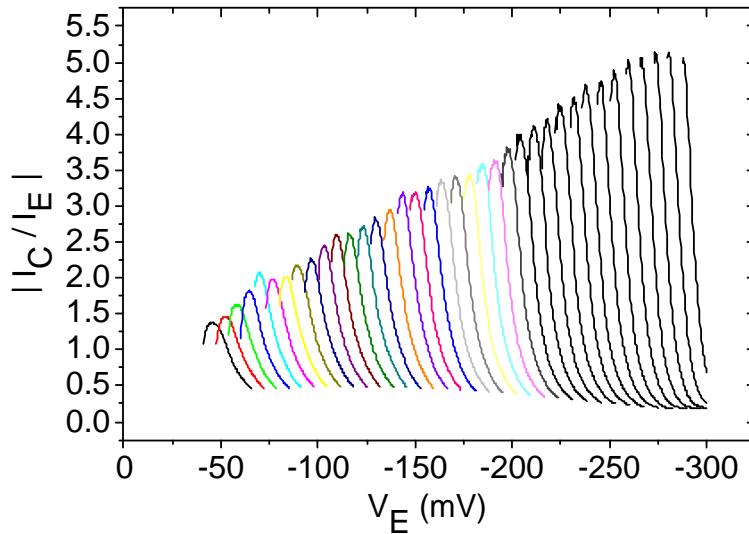
Figure 3.12 : a = | I_C / I_E | versus V_E calculated from selected data from Figure 3.4.;

a has a highest value of 5.5 near V_E = -300 mV. In Ref [1] a ~3 at V_E = -100 mV at 4.2 K. Despite we see a value of 5.5, we can not exceed the value of 3 at injection energy -100 mV. This can be due to etched channel that is used in Ref. [1]; instead we

42

have formed our channel electrostatically. Electron scattering from the walls of etched channel may increase the effect of electron multiplication.

3.2   1.5 K Measurements

There are two physically interesting phenomena in these measurement. Current reversal in base terminal as observed before [1]; and currents reversal at the collector terminal which is a new observation. Due to 1.5 K measurement results, the discussion section is divided in two main parts. The first part is focused on base terminal absolute negative resistance, and the second part is focused on collector absolute negative resistance.
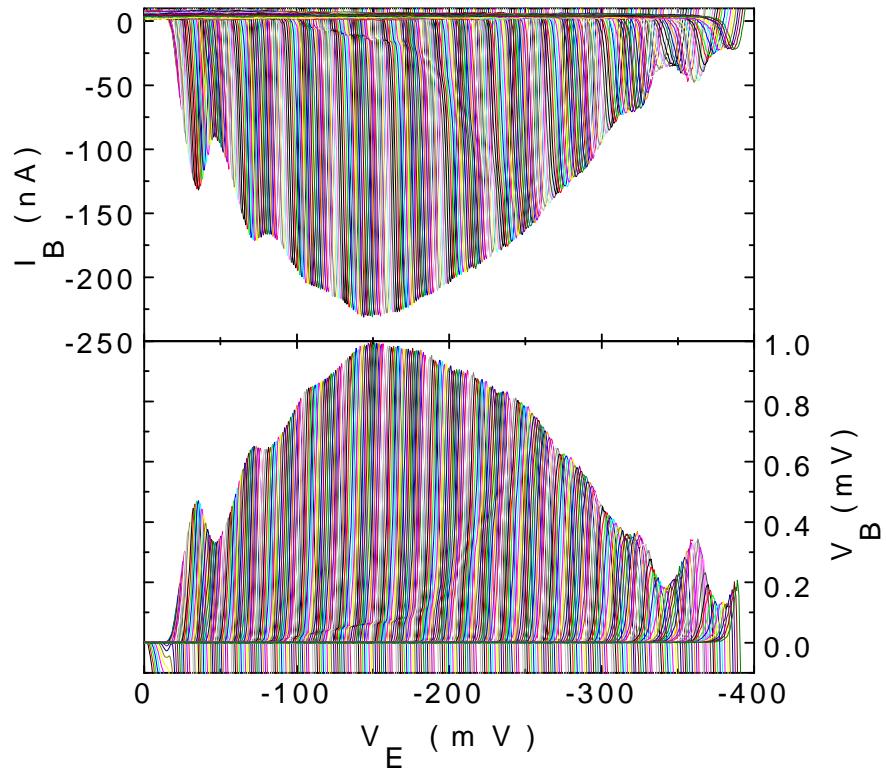
Figure 3.13: I_B and V_B versus V_E at various V_{GE} values at 1.5 K (a) I_B vs V_E; V_{GE} = -400 to -950mV steps: -2mV; V_{GC2} = -362 mV; V_F =-2.2 V; $V_B = V_C = 0$ V; (b) V_B vs V_E; V_{GE} = 0 to -950 mV; V_{GC2}= -362 mV; V_F=-2.2 V; $I_B = 0$ A; $V_C = 0$ V. T = 1.5 K.

3.2.1   Base Terminal Current and Voltage Reversal

In addition to similar measurements of 4.2 K, we have added magnetic field dependence and temperature dependence of base terminal absolute negative resistance.

3.2.1.1 Dependence of Base Current Reversal on Injection Energy

At 1.5 K, dependence of negative I_B on V_{GC2} is shown in Figure 3.13.a. As discussed before, with increasing V_{GE}, electron multiplication shifts to higher injection energies. Three LO-phonon peaks are observed at -36 mV, -72 mV and -108 mV. Thermal peak is seen at -150 mV. There are unexpected peaks at -320 mV and -360 mV. These peaks can be due to higher band excitation of electrons in the structure. Further experimental proof is needed in order to discuss the origin of these peaks.

3.2.1.2. Dependence of Base Potential on Injection Energy at Different Emitter Barrier Heights

In this measurement, I_B is set to zero and V_B is recorded. The result is shown in Figure 3.13.b. Electron multiplication results in a positive potential at the base terminal. The maximum of V_B is 1 mV. The maximum value of V_B was 2 mV in the measurement of 4.2 K. They are not comparable, because in each cooling procedure electronic system may change. In the data of Figure 3.13b, we can also see LO-phonon peaks at -36mV, -72 mV and -106 mV of injection energy. Thermal peak of V_B and thermal peak of I_B are in the same position of V_E. Unexpected peaks at -320 mV and -360 mV are more remarkable in Figure 3.13.b in comparison to Figure 3.13.a.

3.2.1.3 Dependence of Transfer Ratio of Base Negative Current on Injection Energy at Different Emitter Barrier Height

As a next step, transfer ratio $|(I_C / I_E)|$ of electron multiplication is calculated and it is shown in Figure 3.14.b. In comparison to original data, Figure 3.13.a and Figure 3.13.b are put together. In transfer ratio graph, LO-phonon peaks can be seen(-36 mV,

-72 mV and -108 mV). Thermal peak of I_B and thermal peak of transfer ratio $|(I_C / I_E)|$ is not in the same injection energy. Transfer ratio maximum point is at -260 mV of injection energy. But the minimum of I_B is at -160 mV of injection energy. Somehow, heating effect decreases the base current at -160mV, but transfer ratio starts to decrease at -260 mV.
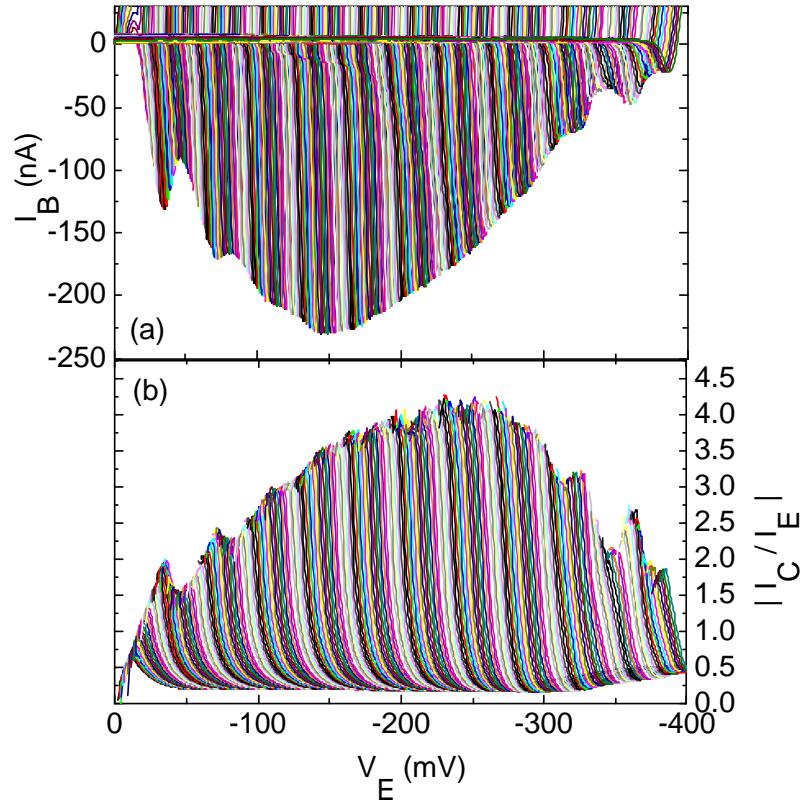
Figure 3.14 :(a) same graph as Figure 3.13.a., same configuration

(b) Calculated transfer ratio $| (I_C / I_E) |$ versus V_E ; from Figure 3.14.a.

Transfer ratio $| (I_C / I_E) |$ maximum has the value of 4 at -260 mV of injection energy. At -100 mV injection energy transfer ratio is 2.5. Additional peaks are seen at -320 mV and -360 mV. It is interesting that these peaks are always in the same position of V_E at Figure 3.14.b, Figure 3.13.a. and Figure.3.13.b.

3.2.1.4 Temperature Dependence

Base terminal potential versus V_E is measured while I_B is set to zero. The data is shown in Figure 3.15. With increasing V_{GE}, positive V_B shifts to higher V_E, and V_B increases as seen in Figure 3.15. Different colors correspond to different temperatures. As seen in the data, with increasing of temperature from 1.5 K to 40 K, V_B decreases monotonically in all values of injection energy. With increasing energy, electron mean free path decreases [3], also acoustic phonons becomes the dominant scattering mechanism [16]. Therefore, electron multiplication mechanism is weakened with increasing temperature. Also as seen in Figure 3.17, peak positions shift with temperature. Mean free path (mfp) of electrons shorten with increasing temperature due to theory [3]. Mean free path also increases with decreasing injection energy. Therefore, in order to have the same mean free path, increase of temperature, results the decrease in injection energy. At the end, we see the same peak at a lower injection energy with increasing temperature.
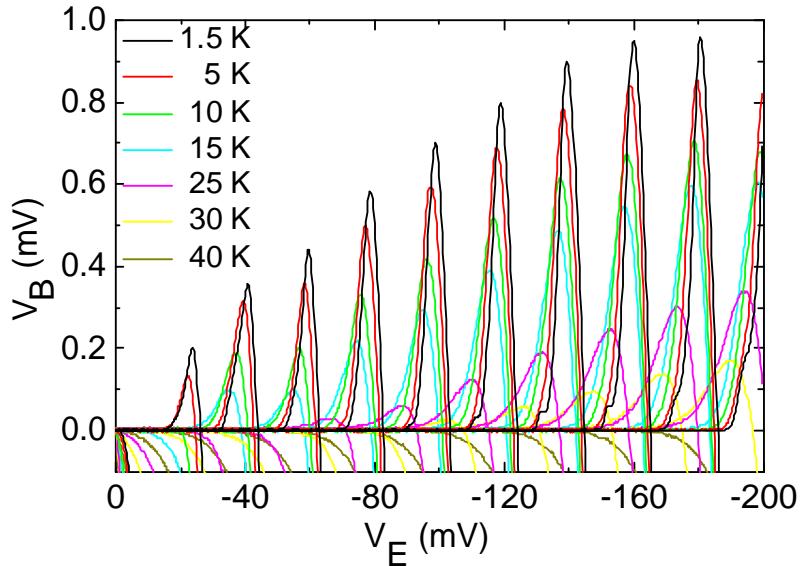
Figure 3.15: Temperature dependence of V_B vs V_E at various V_{GE} values; V_{GE} = -400mV to -700mV in 30mV steps; V_{GC2} is fixed to -362 mV; V_F = -2.2V; I_B = 0 A; V_C = 0 V.

3.2.1.5 Effect of Magnetic Field

Magnetic field dependence of negative I_B versus injection energy is shown Figure 3.16. Different colors refer to different magnetic field values. There are eleven different values of V_{GE}. As explained before, negative I_B value increases with increment of V_{GE}. Magnetic field folds the electrons' trajectory due to Lorentz Force. Also as explained before, electron multiplication is caused by directional scattering. Therefore, magnetic field reduces the probability of scattering electron to reach to collector terminal leading to a monotonic increase of I_B in all magnetic field values. The peak positions do not change significantly because electron mean free is not affected significantly with magnetic field. Also, higher energy electron multiplication is more resistant to magnetic field because scattering electrons at high energy has a higher probability to reach collector terminal, despite they are folded much more than lower energy electrons. We need to calculate the cyclotron radius in order to compare the results of magnetic field dependence.

Cyclotron frequency w_C:

$$w_C = \frac{e\,B}{m^*} \tag{3.1}$$

B is magnetic field strength and r_c is cyclotron radius. From the cyclotron frequency, we can calculate cyclotron radius r_c

$$r_C = v_F \; / \; w_C \tag{3.2}$$

r_C is equal to 1540 nm for 50 mT, 720 nm for 100 mT, 360 nm for 200 mT and 72 nm for 1000 mT.

As seen in the results, cyclotron radius reaches the value base length even at 50 mT. Circular motion of electrons perturbs the directional scattering and hence reduces the negative current.

3.2.2. Collector Terminal Current and Voltage Reversal

In this part the collector current reversal is investigated. Measurements are analogous of section.3.2.1. Dependence of I_C and V_C on V_E and V_{GE} is measured. We have also measured the temperature and magnetic field dependences.

3.2.2.1 Dependence of Collector Current on Injection Energy

Dependence of I_C on V_E at different V_{GE} is measured. The data is shown in Figure 3.17.a. With increasing V_{GE}, I_C peaks shift to higher V_E (see Figure 3.7). Heating effect increases with increasing injection energy. Therefore, the absolute value of I_C increases from -200 mV to -250 mV. Between -250mV to -400mV, electron energy is so high that electron system in the collector region is heated up. Therefore, they heat both base and collector region. Therefore, chemical potential difference between collector and base decreases. This results in the reduction of current reversal from collector.

Unexpected small peaks at -320 mV and -360 mV is also observed in Figure 3.17.a. These peaks are also observed in Figure 3.13.a, Figure 3.13.b, Figure 3.14.a and Figure 3.14.b. These peaks are independent of measurement configuration. These peaks are somehow intrinsic property of structure.

Figure 3.16 : Magnetic Field dependence of I_B vs V_E at various V_{GE} values at 1.5K; V_B = 0 V; V_{GE} = -400 mV to -700 mV with steps -30 mV; V_{GC2} = -362 mV; V_F = -2.2 V.

3.2.2.2 Dependence of Collector Current on Injection Energy

Dependence of I_C on V_E at different V_{GE} is measured. The data is shown in Figure 3.17.a. With increasing V_{GE}, I_C peaks shift to higher V_E (see Figure 3.7). Heating effect increases with increasing injection energy. Therefore, the absolute value of I_C increases from -200 mV to -250 mV. Between -250mV to -400mV, electron energy is so high that electron system in the collector region is heated up. Therefore, they heat both base and collector region. Therefore, chemical potential difference between collector and base decreases. This results in the reduction of current reversal from collector.

Unexpected small peaks at -320 mV and -360 mV is also observed in Figure 3.17.a. These peaks are also observed in Figure 3.13.a, Figure 3.13.b, Figure 3.14.a and Figure 3.14.b. These peaks are independent of measurement configuration. These peaks are somehow intrinsic property of structure.

3.2.2.2. Dependence of Collector Terminal Potential on Injection Energy

V_B is measured when I_B set to zero as described above. V_C versus V_E at different V_{GE} is seen in Figure 3.17.b. The maximum position of V_C is not in the same position of the minimum value of Figure 3.17.a. As discussed before, with increasing injection energy, V_E first increases up to 1 mV at -260mV. This is due to increasing effect of heating. Between -260 mV to -400mV, V_B decreases again due to heating of collector region. Peaks at -320 mV and 360 mV is also seen in this graph. These peaks are seen in the same injection energy at configurations. Therefore, it is most probably intrinsic property of the structure.

3.2.2.3. Temperature Dependence of Collector Potential

As seen in the data (Figure 3.18), V_C does not monotonically decrease with increasing temperature. In the region between -200mV to -280mV, V_C monotonically decreases with increasing injection energy. But in the interval between -280mV to -360 mV, V_C first increases in the 1.5 to 3 K; then starts decreasing. This result shows that there is a different type of transport in the region. Also this is the same region that we

observe the unexpected peak (320 mV and 360mV). Further theoretical work is needed to explain this phenomena.

3.2.2.4. Magnetic Field Dependence of Collector Current Reversal

As shown in Figure 3.19, magnetic field dependence of negative I_C is measured at different V_{GE}. As shown in the figure, absolute value of I_C decreases with increasing magnetic field. There is a monotonic decrease of absolute value of I_C with increasing magnetic field. Magnetic field dependence of I_C is significantly higher than magnetic field dependence of I_B. The reason of negative I_B is directional scattering. The reason of negative I_C is heating of base region. Therefore, it is expected that I_B would have
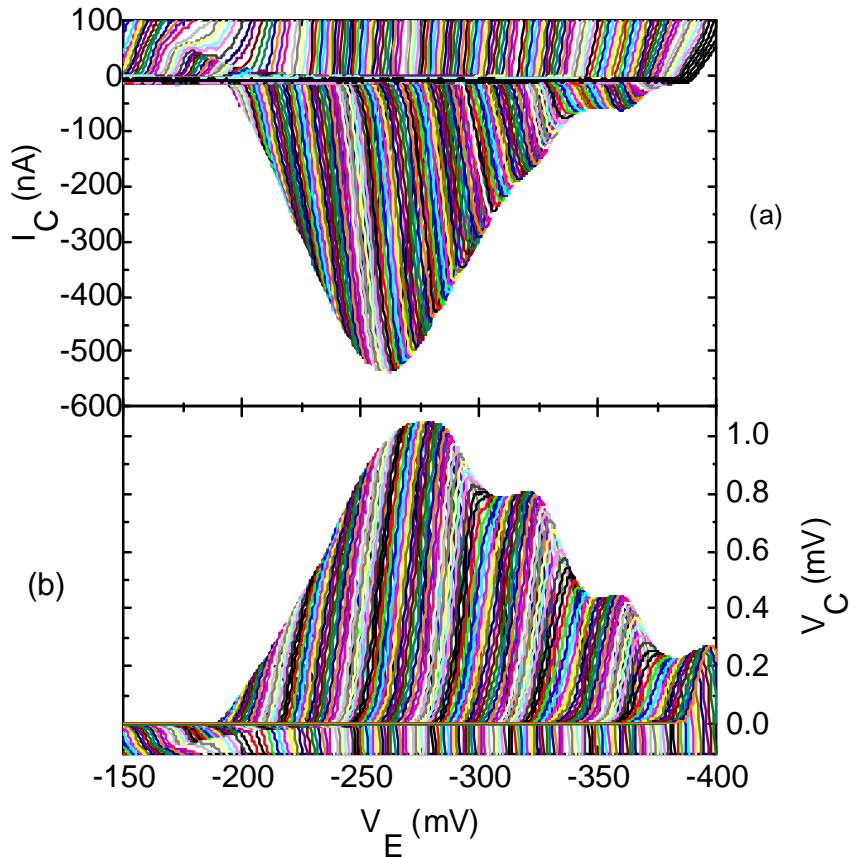
Figure 3. 17: I_C and V_C versus V_E at various V_{GE} values at 1.5 K ; (a) I_C vs V_E ; $V_{GE} = $ -620 mV to -950 mV steps -30 mV; $V_{GC2} = $ -235 mV; V_F is biased to -2.2 V; $V_C = V_B = 0$ V. (b) V_C vs V_E at $I_C = 0$ A; $V_{GE} = $ -620 mV to -950 mV in 30mV steps; $V_{GC2} = $ -235 mV; V_F is biased to -2.2V; $V_B = 0$ V.

higher magnetic field dependence. But the experimental results show the opposite. Further experimental and theoretical study is needed in order to explain this conflict.
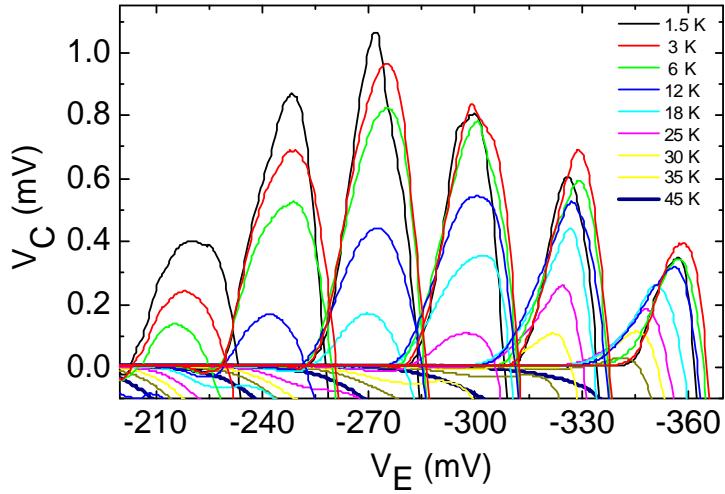
Figure 3.18 : Temperature dependence of V_C versus V_E at various V_{GE} values at 1.5 K; $I_C = 0$ nA; V_{GE} is -700 mV to -900 mV with steps -40 mV; $V_{GC2} = -235$ mV; $V_F = -2.2$V .
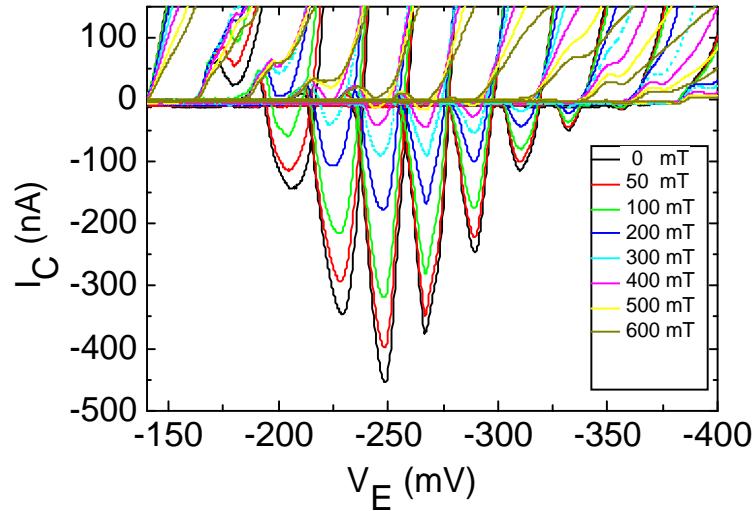
Figure 3.19: Magnetic field dependence of I_C versus V_E at various V_{GE} values at 1.5 K ;$V_C = 0$; $V_{GE} = -620$mV to -950 mV with steps: -33 mV; $V_{GC2} = -235$mV; $V_F = 2.2$V;

Chapter 4

CONCLUSION

A novel electron-electron scattering device with 2 µm base length is fabricated. Current reversal in the base terminal is directional scattering and it is observed at 4.2 K. Moreover, a current reversal in the collector terminal is observed and attributed to the heating of the electronic system. Transfer ratio of the device ($| IC / IE| $) becomes 5 at -300mV emitter injection. Compared to previous results with 5 µm base length, the current transfer ratio is not enhanced. This difference can be connected to the etched channel of 2DEG. The explanation needs further analysis of data and possibly new measurements.

Results of 4.2 K measurements and their discussions lead to further investigation of the absolute negative resistance of the base terminal and collector terminal at 1.5 K. Discussion of results at 1.5 K gives birth to a lot of open questions. Further theoretical and experimental studies are needed in order to explain the results.

Unexpected current reversal of collector terminal is more dependent to magnetic field than the reversal current of base terminal. Current reversal effect at collector terminal can be seen up to 35 K. Transfer ratio of collector negative current $| I_B / I_E |$ has a maximum value of 2.8. Further experimental studies are essential to explain transfer ratio and temperature dependence of negative collector current.

Optical phonon peaks are observed at injection energy of -36mV, -72mV and -108mV both at base terminal and at collector terminal current/voltage measurements. However, there are additional peaks observed at injection energies of 327 meV and 365 meV. Further analysis is needed to understand the origin of these unexpected peaks.

Bibliography

[1]   I. I. Kaya and K. Eberl, "Absolute Negative Resistance Induced by Directional Electron-Electron Scattering in a Two-Dimensional Electron Gas", submitted to Physical Review Letters, (July 4, 2006)

[2]   I. I. Kaya, "Hot Electron Interactions in Nanostructures" , Phd Thesis, Bilkent University, Physics Department, February 1997.

[3]   Gabrielle F. Giuliani and John J. Quinn, "Lifetime of a quasiparticle in a two-dimensional electron gas" , Physical Review B , Volume 26 , Number 8 , pg 4421 (1982)

[4]   H. Buhmann, R. N. Gurzi, A. N. Kalinenko, A. I. Kopeliovich, L. W. Molenkamp, A. V. Yanovsky,   "On Electron-Electron Scattering Mechanisms in 2D Degenerated Systems " , Nanostructured Materials, Vol 12, pg 835-838, (1999)

[5]   R. N. Gurzhi, A.N.Kalinenko, and A. I. Kopeliovich, "Electron-electron momentum relaxation in a two-dimensional electron gas", Physical Review B, Volume 52, Number 7, pg 4744, (1995)

[6]   R. Dingle, H. L. Stormer, A. C. Gossard and W. Wiegman, "Electron mobilities in modulation-doped semiconductor heterojunction superlattice" , Applied Physics Letter, 33 (7) , 665 (1978)

[7]   Introduction to Modern Solid State Physics , Yuri M. Galperin

[8]   Marvin L. Cohen and T. K. Bergstresser, "Band Structures and Pseudopotential Form Factors for Fourteen Semiconductors of the Diamond and Zinc-blende Structures" , Physical Review, Volume 141, Number 2, 789, 1966

[9]   U. Sivan, M. Heiblum, C. P. Umbach, H. Shtrikman, "Electrostatic electron lens in the ballistic regime", Physical Review B, Volume 41, Number 11, (1990) pg 7937

[10]   J. Spector , H.L. Stormer, K. W. Baldwin, L. N. Pfeifer and K. W. West, "Control of ballistic electrons in macroscopic two-dimensional electron systems." , Appl. Phys. Lett, 56 (13) (1990) pg 1290

[11]   L. W. Molenkamp, A. A. M. Staring , C. W. J. Beenakker, R. Eppenga, C. E. Timmering and J. G Williamson, C.J. P. M. Harmans, C. T. Foxon, "Electron-

beam collimation with a quantum point contact", Physical Review B, Volume 41, Number 2, pg 1274

[12] B. J. van Wees, H. van Houten, C. W. J. Beenaker, J. G. Williamson, L. P. Kouwenhoven, D. Van der Marel, C. T. Foxon, "Quantized Conductance of Point Contacts in a Two-Dimensonal Electron Gas" , Physical Review Letters, Volume 60, Number 9, (1988) , pg 848

[13] U. Sivan, M. Heiblum, and C. P. Umbach, " Hot Ballistic Transport and Phonon Emission in a Two-Dimensional Electron Gas " , Physical Review Letters, Volume 63, Number 9, pg 992, (1989)

[14] B.Laikhtman, U. Sivan, A. Yacoby, C. P. Umbach, M. Heiblum, J. A. Kash, and Shtrikman, " Long Mean Free Path of Hot Electrons Selectively Injected to Higher Subbands " , Physical Review Letters, Volume 65, Number 17, pg 2181, (1990)

[15] Kiyoyuki Yokoyama and Karl Hess, "Monte Carlo study of electronic transport in $Al_{1-x} Ga_x$ As / GaAs single-well heterostructures." , Physical Review B, Volume 33, Number 8, 5595 (1986)

[16] T. Kawamura and S. Das Sarma, "Phonon-scattering-limited electron mobilities in $Al_xGa_{1-x}As$ / GaAs heterojunction." , Physical Review B, Volume 45, Number 7, pg 3612 (1992)

[17] Kazuhiko Hirakawa and Hiroyuki Sakaki, "Mobility of the two-dimensional electron gas at selectively doped n -type $Al_xGa_{1-x}As$/GaAs heterojunctions with controlled electron concentrations" , Physical Review B, Volume 33, Number 12, 8291, (1986)

[18] Loren Pfeiffer, K. W. West, H. L. Stormer and K. W. Baldwin, "Electron mobilities exceeding 10^7 cm^2 / V.s in modulation-doped GaAs." , Appl. Phys. Lett. , 55 (18) (1989)

[19] L.W. Molenkamp and M.J.M. de Jong, " Electron-electron-scattering induced size effects in a two-dimensional wire" , Physical Review B, 49, Number 7, (1994)

[20] L.W. Molenkamp, M. J. Brugmans, H. Van Houten and C. T. Foxon, "Electron—electron scattering probed by a collimated electron beam" , Semicon. Sci. Technol. 7 , (1992) B228-B230

[21] R. Gurzhi, A. I. Kopeliovich, A.N. Kalinenko, A. V. Yanovsky, E. N. Bogachek, Uzi Landman, H. Buhmann, L. W. Molenkamp, "Relaxation of high-energy quasiparticle distributions: Electron-electron scattering in a two dimensional electron gas." , Physical Review B, 68, 165318, (2003)

[22] F. Müller, B. Lengeler, Th. Schalpers, J. Appenzeller, A. Förster, Th. Klocke, and H. Lüth, "Electron-electron interaction in ballistic electron beams." , Physical Review B, Volume 51, Number 8, (1995)

[23]   M. J. de Jong, and L. W. Molenkamp, "Hydrodynamic electron flow in high mobility wires. " , Physical Review B, Volume 51, Number 16, 13389, (1995)

[24]   H. Predel, H. Buhmann, , L. W. Molenkamp, R. N. Gruzhi, A. N. Kalinenko, A. I. Kopeliovich and A. Yanovsky, " Effects of electron-electron scattering on electron-beam propagation in a two-dimensional electron gas." , Physical Review B, Volume 62, Number 3, 2057, (2000)

[25]   A. Yacoby, U. Sivan, C. P. Umbach and J. M. Hong, " Interference and Dephasing by Electron-Electron Interaction on Length Scales Shorter than the Elastic Mean Free Path " , Physical Review Letters, Volume 66, Number 14, 1938, (1991)

[26]   H. Fukuyama and E. Abrahams, Physical Review B, 27 , 5976, (1983)

[27]   S. Q. Murphy, J. P. Eisenstein, L. N. Pfeifer, and K. W. West, " Lifetime of two-dimensional electrons measured by tunneling spectroscopy." , Phys. Rev. B. 52, 14 825 (1995)

[28]   Lian Zheng and S. Das Sarma , " Coulomb scattering lifetime of two-dimensional electron gas. " , Physical Review B , Volume 53 , Number 15 , pg 9964 (1996)

[29]   H. Predel, H. Buhmann, L.W. Molenkamp, Physical Review B, Volume 62, Numver 3, pg 2057, (2000)

[30]   A. V. Yanovsky, H. Predel, H. Buhmann, R. N. Gurzhi, A. N. Kalinenko, A. I. Kopeliovich, L. W. Molenkamp, "Spectroscopical imaging of electron scattering in two-dimensional conductors." , Physica E 12, pg 241-243, (2002)

[31]   H. Buhmann, R. N. Gurzhi, A. N. Kalinenko, A. I. Kopeliovich, L. W. Molenkamp, H. Predel, A. V. Yanovsky, "New transport effects in a degenerate two-dimensional electron gas." , Physica B, 284-288, pg 1904-1905, (2000)

[32]   H. Buhnmann, H. Predel, L. W. Molenkamp, R. N. Gurzhi, A. I. Kopeliovich, A. N. Kalinenko, A. V. Yanovsky, "Electron-electron scattering and the propagation of electron beams in a two-dimensional electron gas." , Physica E 6, pg 310-313, (2000)

[33]   R. N. Gurzhi, A. N. Kalinenko, A.I. Kopeliovich, "Electron-electron momentum relaxation in a two-dimensional electron gas." , Physical Review B, Volume 52, Number 7, pg 4744, (1995)

[34]   H. Buhmann, R. N. Gurzhi, A.N. Kalinenko, A. I. Kopeliovich, L. W. Molenkamp, A. V. Yanovsky, Nanostructured Materials, Vol 12, pp 835-838, 1999.

[35]   A.Palevski, M. Heiblum, C. P. Umbach, C. M. Knoedler, A. N. Broers, and R. H. Koch, " Lateral Tunneling, Ballistic Transport and Spectroscopy in a Two-dimensional electron Gas. " , Physical Review Letters, Volume 62, Number 15

[36]   W. Fawcett, A. D. Boardman, and S. Swain, J. Phys. Chem. Solids, 31, 1963 (1970)

[37]   P. H. Hawyark, G. Eliasson and J. J. Quinn, Physical Review B, 37, 10187, (1988)

[38]   B.Brill and M. Heiblum, Physical Review B, Volume 49, Number 20, (1994)

[39]   M. W. Dellow, N. J. Cronin, and S.J. Bending, " Tunneling hot electron transistor as a high power source at terahertz frequencies " , Appl. Phys. Lett. 65, (19), (1994)

[40]   I. I. Kaya, M.W. Dellow, S.J.Bending, E. H. Linfield, P. D. Rose, D. A. Ritchie and G.A.C. Jones, "In-situ focused ion beam implantation for the fabrication of a hot electron transistor oscillator structure. " , Semicond. Sci. Technology, 11, (1996), 135-138

[41]   A. O. Govorov and J. J. Heremans, "Hydrodynamic Effects in Interacting Fermi Electron Jets." , Phys. Rev. Lett., 92, 026803, (2004)

[42]   Davies J. H., "The physics of low dimensional semiconductors", Cambridge University Press, 1998